Current Status of GW Detection

Wei-Tou Ni 倪维斗
National Tsing Hua University

Refs: (i) S. Kuroyanagi, L-W Luo and WTN, GW sensitivities over all frequency band

(ii) K Kuroda, WTN, WP Pan, IJMPD 24 (2015) 1530031

(iii) LIGO/Virgo Collaborations, GWTC-1: A GW Transient Catalog of Compact Binary Mergers Observed by LIGO and Virgo O1 & O2

(iv) LIGO/Virgo Collaborations, BBH Population Properties Inferred from O1 & O2 Observing Runs

(v) WTN, GW detection in space IJMPD 25 (2016) 1530002 ………

Among other things, 20th Century will be memorized by the advancement of fundamental physical theory and the experimental precision

- 1915 General Relativity, 1916 Gravitational Waves (Einstein)
- Early 1900's: Strain Measurement precision → 10^{-6}
- 1960's: Strain Measurement precision → 10^{-16}

  Weber Bar (50 Years ago) 10 orders of gap abridged

- Cryogenic Resonators; Laser Interferometry

- Early 2000's: Strain Measurement precision → 10^{-21}
- 2015: 10^{-22} strain precision on Detection of GWs

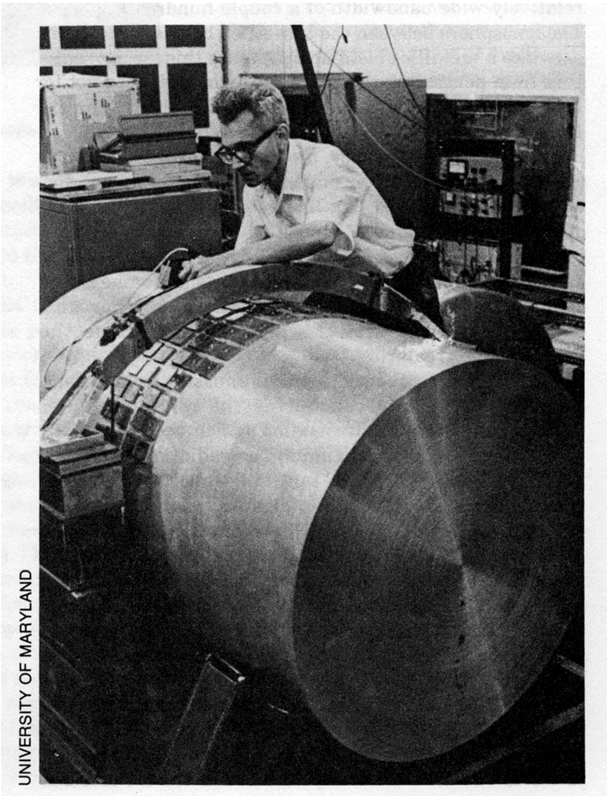

Ground-based GW detectors

KAGRA

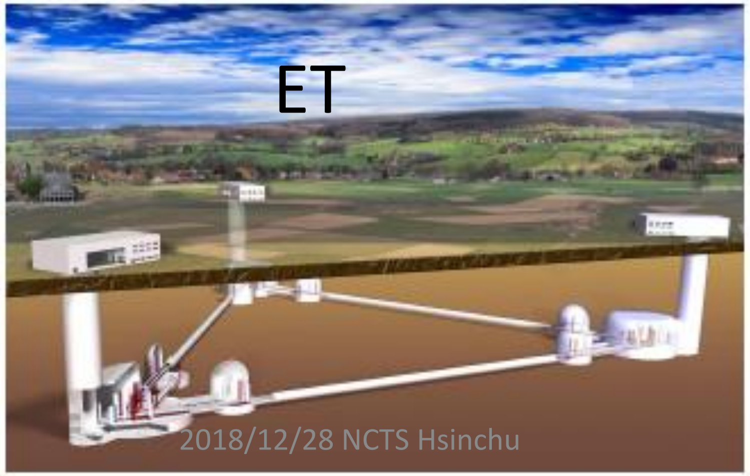

2016 February 11 Announcement of first (direct) detection of Black Holes and GWs

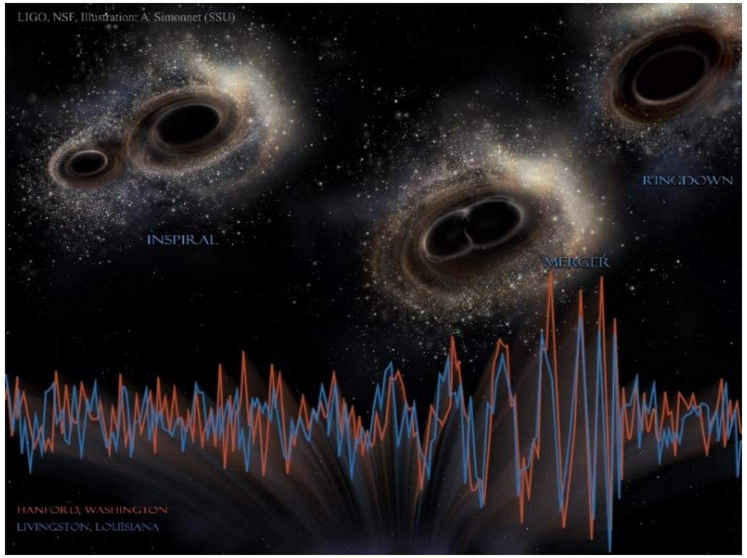

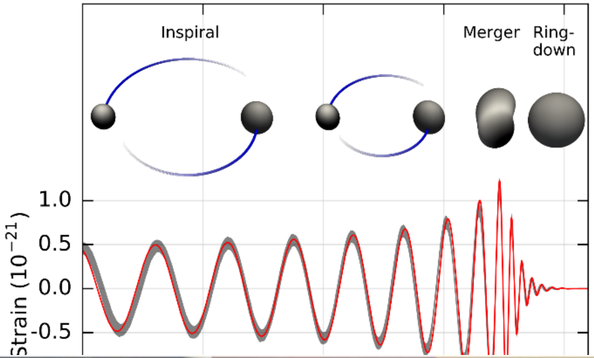

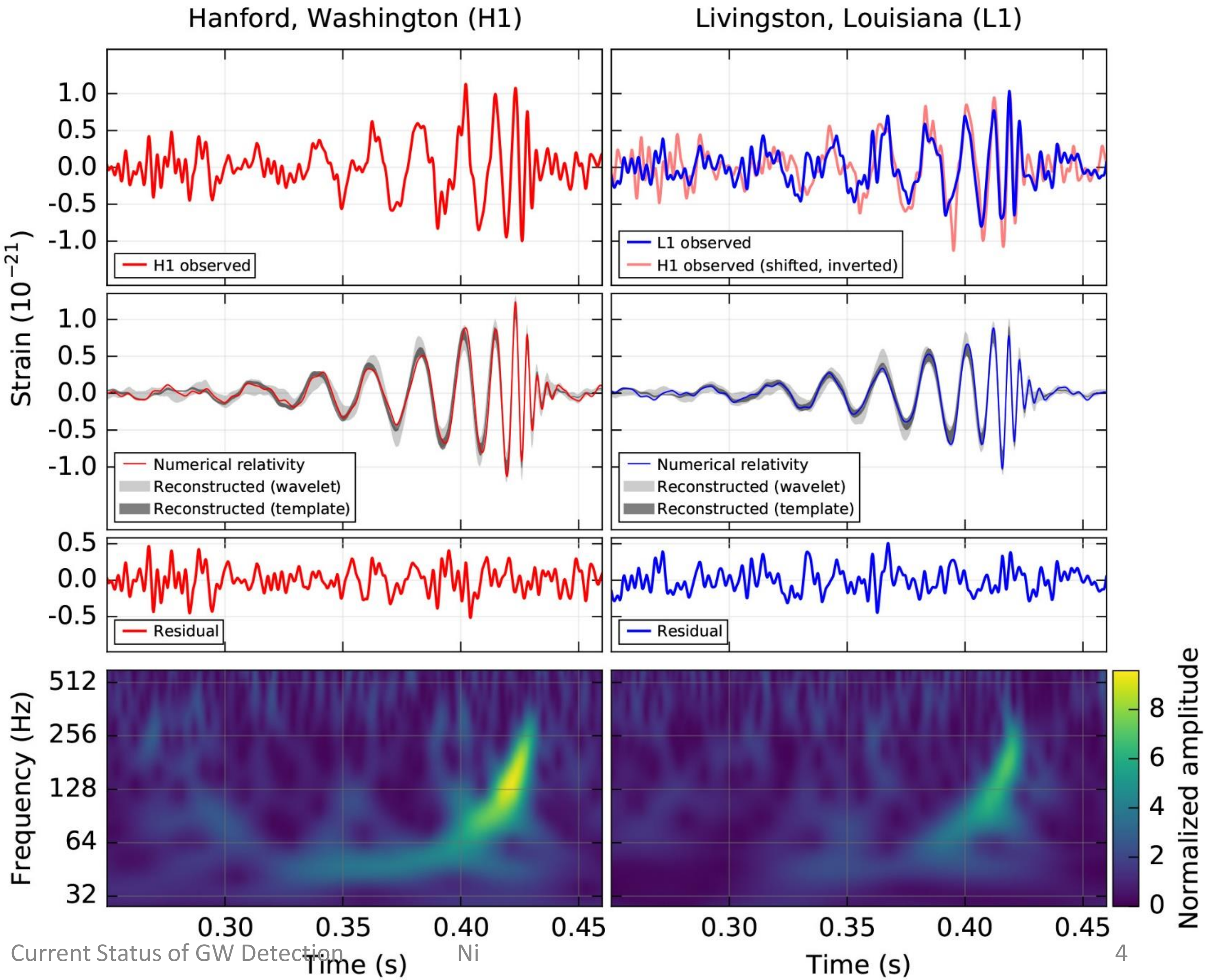

2017.08.17 NSB coalescence, ApJ 848

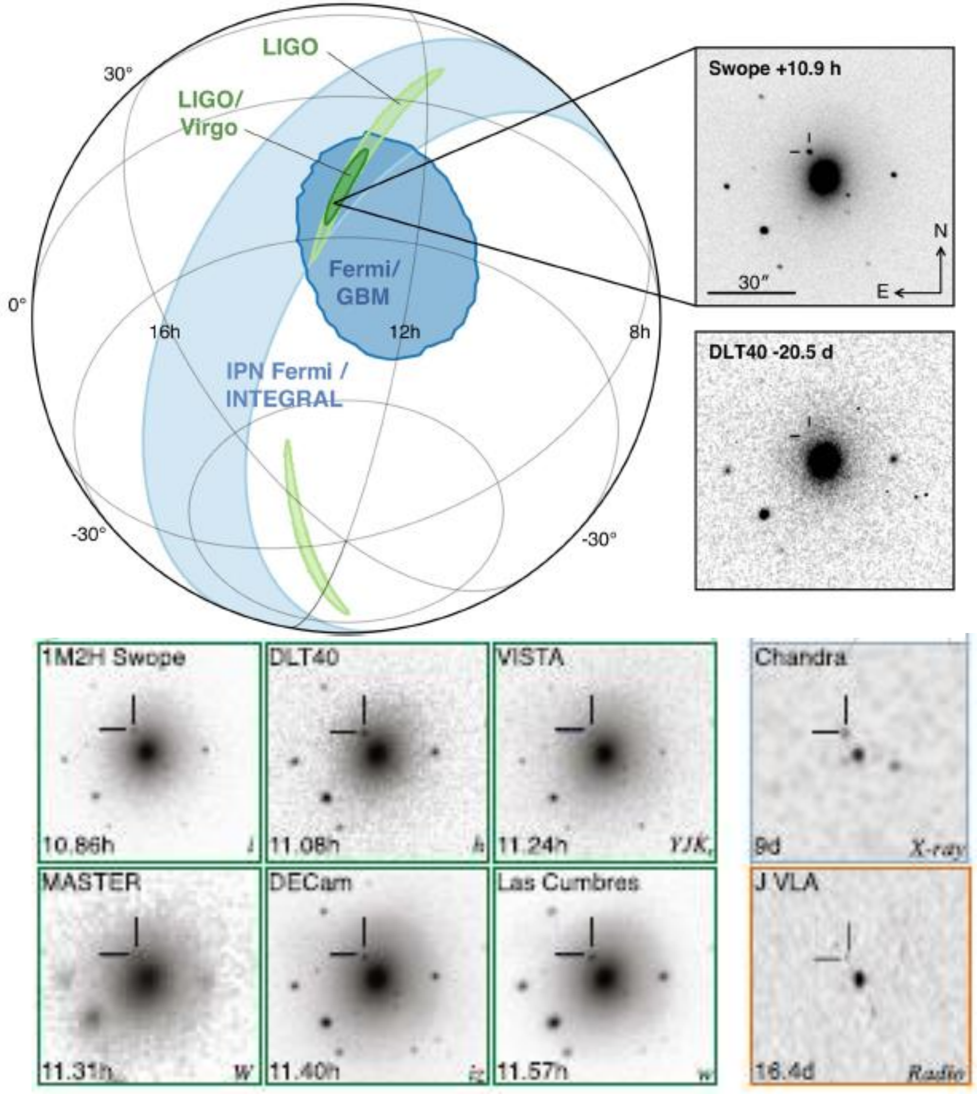

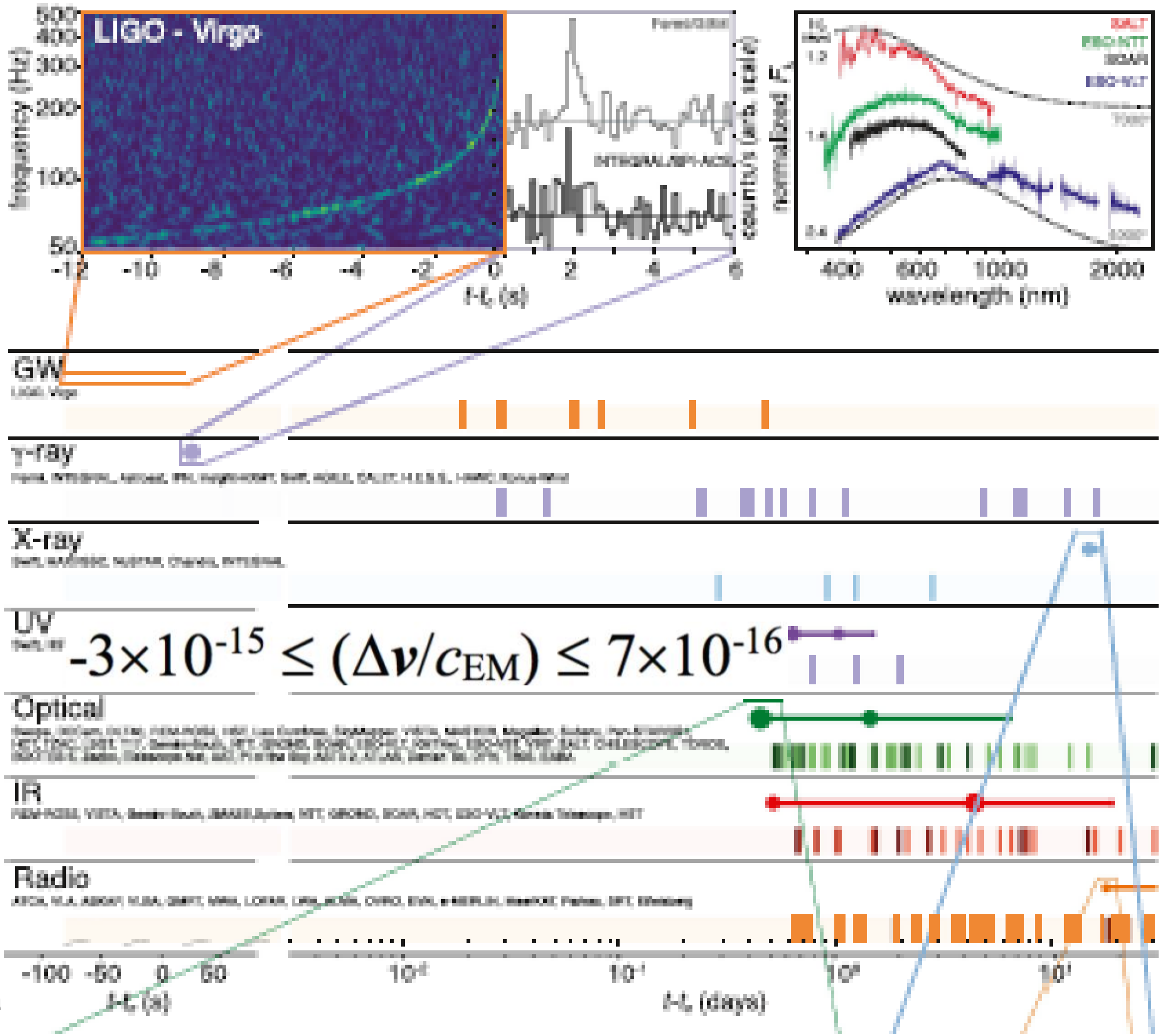

$$-3\times10^{-15} \leq (\Delta v/c_{EM}) \leq 7\times10^{-16}$$

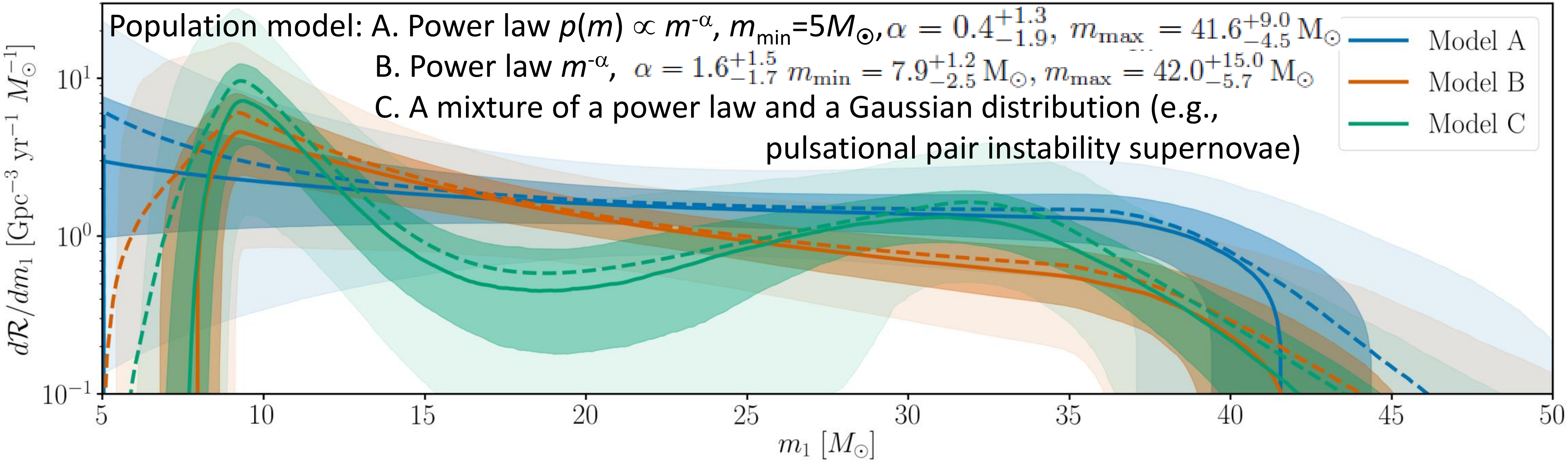

2016-17 announced

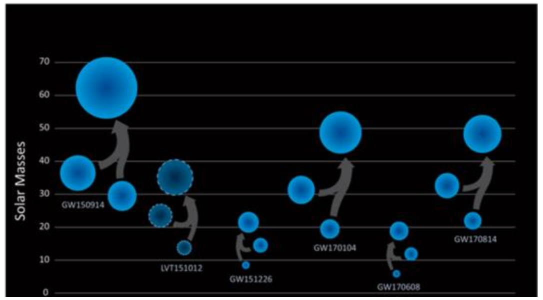

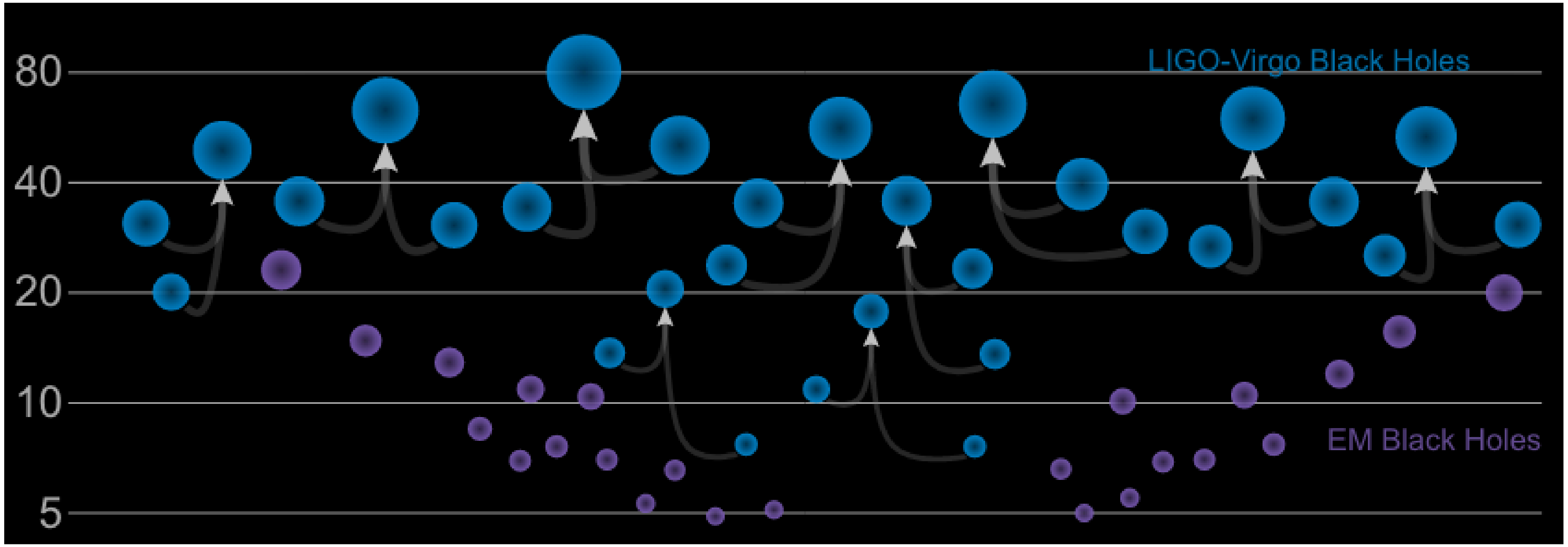

LIGO-VIRGO BHs (7-80 $M_\odot$) + EM observed BHs (5-25 $M_\odot$)

Event Rates

- Binary Black Holes: After the detection of GW170104
- Between 12-213 $Gpc^{-3}\ y^{-1}$
- Including all O1 & O2 events
- power law distribution
- 56^{+44}_{-27} $Gpc^{-3}\ y^{-1}$ (GstLAL)
- 57^{+47}_{-29} $Gpc^{-3}\ y^{-1}$ (PyCBC)
- uniform in log distribution
- $18.1^{+13.9}_{-8.7}$ $Gpc^{-3}\ y^{-1}$ (GstLAL)
- $19.5^{+15.2}_{-9.7}$ $Gpc^{-3}\ y^{-1}$ (PyCBC)
- Neutron Star Binaries: (uniform mass set)
- 662^{+1609}_{-565} $Gpc^{-3}\ y^{-1}$ (GstLAL)
- 800^{+1970}_{-680} $Gpc^{-3}\ y^{-1}$ (PyCBC)

Left: BNS range for each instrument during O2. The break at week 3 was for the 2016 end-of-year holidays. There was an additional break in the run at week 23 to make improvements to instrument sensitivity. The Montana earthquake's impact on the LHO instrument sensitivity can be seen at week 31. Virgo joined O2 in week 34.
Right: Amplitude spectral density of the total strain noise of the Virgo, LHO and LLO detectors. The curves are representative of the best performance of each detector during O2.

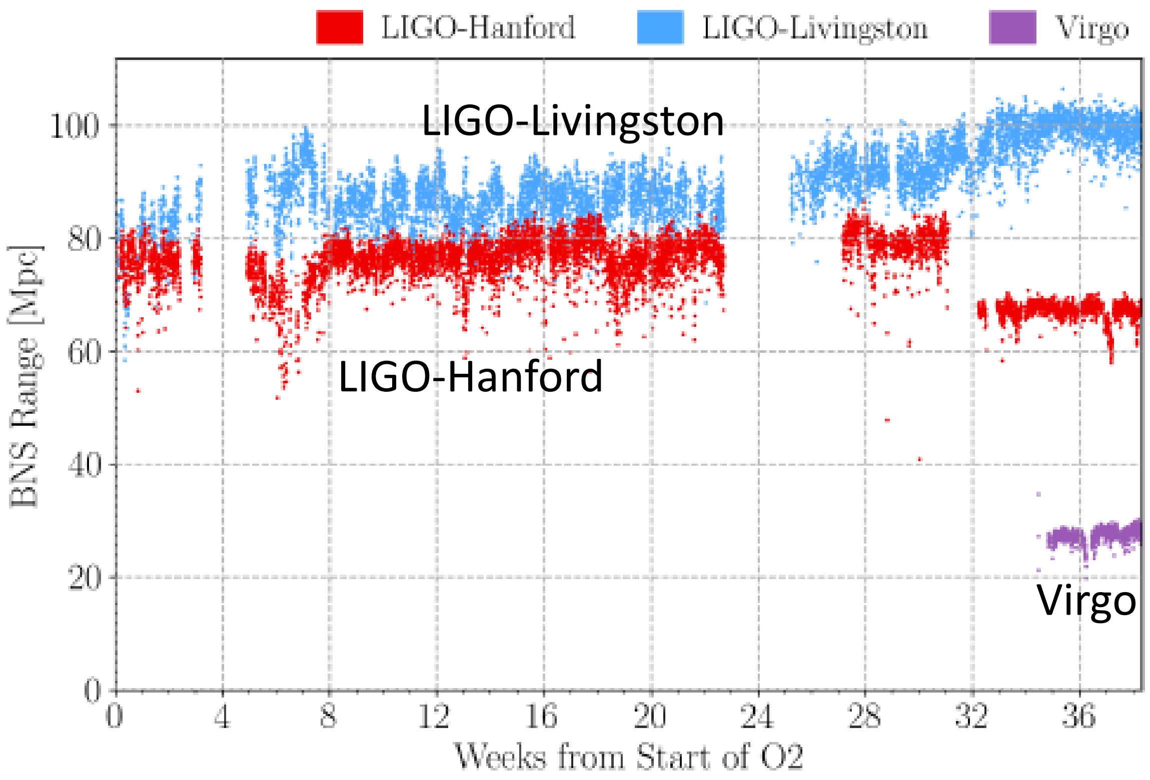

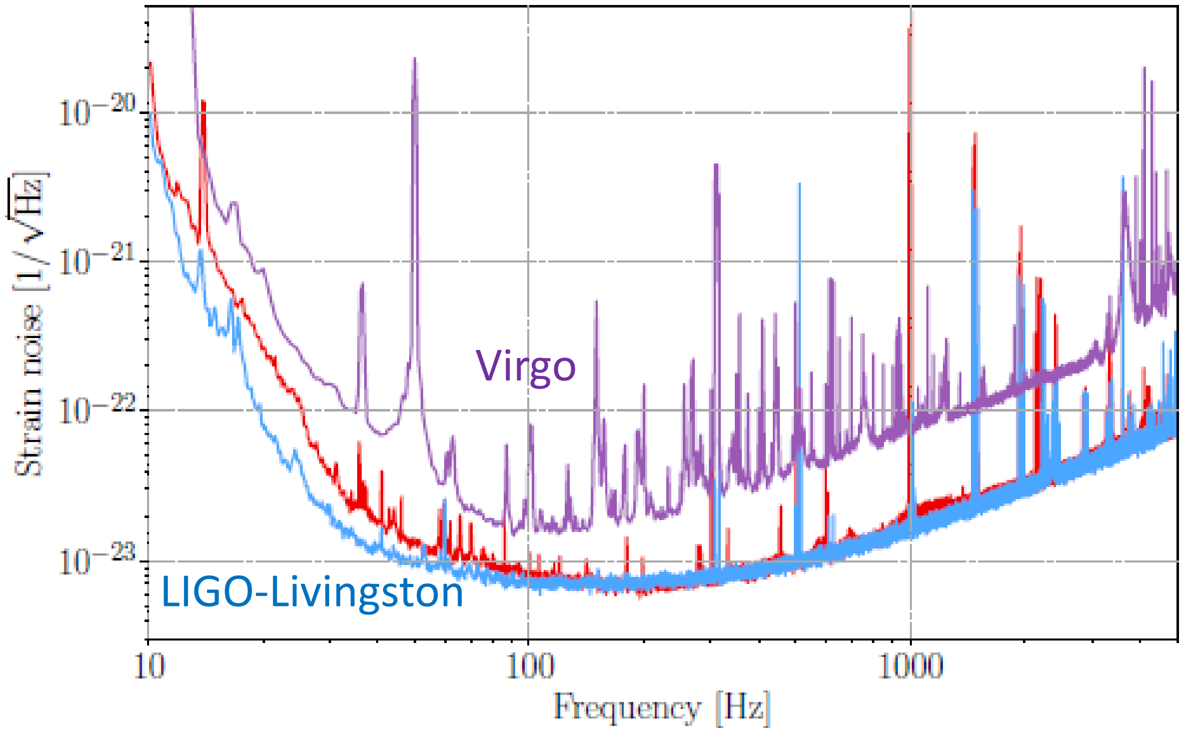

3 Search Pipelines: PyCBC, GstLAL, Coherent WaveBurst (cWB)

- PyCBC – Python Compact Binary Coalescence (an open source software package primarily written in the Python programming language which is designed for use in GW data analysis): direct matched filtering of data against a bank of template waveforms to calculate the SNR for each combination of detector, template waveform and coalescence time.
- GstLAL -- a gravitational-wave search pipeline based on the GstLAL library [14], and derived from GStreamer [15] and the LIGO Algorithm Library [16].
- [14] \Gstlal," https://www.lsc-group.phys.uwm.edu/daswg/projects/gstlal.html, accessed: 2015-07-01.
- [15] \Gstreamer," https://gstreamer.freedesktop.org.
- [16] \Lalsuite," https://www.lsc-group.phys.uwm.edu/daswg/projects/lalsuite.html, accessed: 2015-07-01.
- Coherent WaveBurst (cWB) is an analysis algorithm used in searches for weakly modeled (or unmodeled) transient signals with networks of GW detectors. Designed to operate without a specific waveform model, cWB identifies coincident excess power in the multi-resolution time-frequency representations of the detector strain data [79], for signal frequencies up to 1 kHz and durations up to a few seconds.

Search results for the eleven GW events. We report a false-alarm rate for each search that found a given event; otherwise, we display '–'. The network SNR for the two matched filter searches is that of the template ranked highest by that search, which is not necessarily the template with the highest SNR. Moreover, the network SNR is the quadrature sum of the detectors coincident in the highest-ranked trigger; in some cases, only two detectors contribute, even if all three were operating nominally at the time of that event.

		FAR [y^{-1}]			Network SNR		
Event	UTC Time	PyCBC	GstLAL	cWB	PyCBC	GstLAL	cWB
GW150914	09:50:45.4	$< 1.53 \times 10^{-5}$	$< 1.00 \times 10^{-7}$	$< 1.63 \times 10^{-4}$	23.6	24.4	25.2
GW151012	09:54:43.4	0.17	7.92×10^{-3}	–	9.5	10.0	–
GW151226	03:38:53.6	$< 1.69 \times 10^{-5}$	$< 1.00 \times 10^{-7}$	0.02	13.1	13.1	11.9
GW170104	10:11:58.6	$< 1.37 \times 10^{-5}$	$< 1.00 \times 10^{-7}$	2.91×10^{-4}	13.0	13.0	13.0
GW170608	02:01:16.5	$< 3.09 \times 10^{-4}$	$< 1.00 \times 10^{-7}$	1.44×10^{-4}	15.4	14.9	14.1
GW170729	18:56:29.3	1.36	0.18	0.02	9.8	10.8	10.2
GW170809	08:28:21.8	1.45×10^{-4}	$< 1.00 \times 10^{-7}$	–	12.2	12.4	–
GW170814	10:30:43.5	$< 1.25 \times 10^{-5}$	$< 1.00 \times 10^{-7}$	$< 2.08 \times 10^{-4}$	16.3	15.9	17.2
GW170817	12:41:04.4	$< 1.25 \times 10^{-5}$	$< 1.00 \times 10^{-7}$	–	30.9	33.0	–
GW170818	02:25:09.1	–	4.20×10^{-5}	–	–	11.3	–
GW170823	13:13:58.5	$< 3.29 \times 10^{-5}$	$< 1.00 \times 10^{-7}$	2.14×10^{-3}	11.1	11.5	10.8

Marginal triggers from the two matched-filter CBC searches. The search that identified each trigger is given, and the false alarm and network SNR. This network SNR is the quadrature sum of the individual detector SNRs for all detectors involved in the reported trigger; that can be fewer than the number of nominally operational detectors at the time, depending on the ranking algorithm of each pipeline. The detector chirp mass reported is that of the most significant template of the search. The final column indicates whether there are any detector characterization concerns with the trigger; for an explanation and more details, see the text.

Date	UTC	Search	FAR [y^{-1}]	Network SNR	$\mathcal{M}^{det}$ [$M_\odot$]	Data Quality
151008	14:09:17.5	PyCBC	10.17	8.8	5.12	No artifacts
151012A	06:30:45.2	GstLAL	8.56	9.6	2.01	Artifacts present
151116	22:41:48.7	PyCBC	4.77	9.0	1.24	No artifacts
161202	03:53:44.9	GstLAL	6.00	10.5	1.54	Artifacts can account for
161217	07:16:24.4	GstLAL	10.12	10.7	7.86	Artifacts can account for
170208	10:39:25.8	GstLAL	11.18	10.0	7.39	Artifacts present
170219	14:04:09.0	GstLAL	6.26	9.6	1.53	No artifacts
170405	11:04:52.7	GstLAL	4.55	9.3	1.44	Artifacts present
170412	15:56:39.0	GstLAL	8.22	9.7	4.36	Artifacts can account for
170423	12:10:45.0	GstLAL	6.47	8.9	1.17	No artifacts
170616	19:47:20.8	PyCBC	1.94	9.1	2.75	Artifacts present
170630	16:17:07.8	GstLAL	10.46	9.7	0.90	Artifacts present
170705	08:45:16.3	GstLAL	10.97	9.3	3.40	No artifacts
170720	22:44:31.8	GstLAL	10.75	13.0	5.96	Artifacts can account for

Selected source parameters of the eleven confident detections. We report median values with 90% credible intervals that include statistical errors, and systematic errors from averaging the results of two waveform models for BBHs. For GW170817 credible intervals and statistical errors are shown for IMRPhenomPv2NRT with low spin prior, while the sky area was computed from TaylorF2 samples. The redshift for NGC 4993 from [87] and its associated uncertainties were used to calculate source frame masses for GW170817. For BBH events the redshift was calculated from the luminosity distance and assumed cosmology as discussed in Appendix B. The columns show source frame component masses mi and chirp mass $\mathcal{M}$, imensionless effective aligned spin X_{eff} , final source frame mass M_{f} , final spin a_{f} , radiated energy E_{rad}, peak luminosity l_{peak}, luminosity distance d_{L}, redshift z and sky localization $\Delta\Omega$. The sky localization is the area of the 90% credible region. For GW170817 we give conservative bounds on parameters of the final remnant discussed in Sec. VE.

Event	$m_1/\mathrm{M}_\odot$	$m_2/\mathrm{M}_\odot$	$\mathcal{M}/\mathrm{M}_\odot$	χ_{eff}	$M_{\mathrm{f}}/\mathrm{M}_\odot$	a_{f}	$E_{\mathrm{rad}}/(\mathrm{M}_\odot c^2)$	$\ell_{\mathrm{peak}}/(\mathrm{erg\,s^{-1}})$	d_L/Mpc	z	$\Delta\Omega/\mathrm{deg}^2$
GW150914	$35.6^{+4.8}_{-3.0}$	$30.6^{+3.0}_{-4.4}$	$28.6^{+1.6}_{-1.5}$	$-0.01^{+0.12}_{-0.13}$	$63.1^{+3.3}_{-3.0}$	$0.69^{+0.05}_{-0.04}$	$3.1^{+0.4}_{-0.4}$	$3.6^{+0.4}_{-0.4}\times 10^{56}$	430^{+150}_{-170}	$0.09^{+0.03}_{-0.03}$	179
GW151012	$23.3^{+14.0}_{-5.5}$	$13.6^{+4.1}_{-4.8}$	$15.2^{+2.0}_{-1.1}$	$0.04^{+0.28}_{-0.19}$	$35.7^{+9.9}_{-3.8}$	$0.67^{+0.13}_{-0.11}$	$1.5^{+0.5}_{-0.5}$	$3.2^{+0.8}_{-1.7}\times 10^{56}$	1060^{+540}_{-480}	$0.21^{+0.09}_{-0.09}$	1555
GW151226	$13.7^{+8.8}_{-3.2}$	$7.7^{+2.2}_{-2.6}$	$8.9^{+0.3}_{-0.3}$	$0.18^{+0.20}_{-0.12}$	$20.5^{+6.4}_{-1.5}$	$0.74^{+0.07}_{-0.05}$	$1.0^{+0.1}_{-0.2}$	$3.4^{+0.7}_{-1.7}\times 10^{56}$	440^{+180}_{-190}	$0.09^{+0.04}_{-0.04}$	1033
GW170104	$31.0^{+7.2}_{-5.6}$	$20.1^{+4.9}_{-4.5}$	$21.5^{+2.1}_{-1.7}$	$-0.04^{+0.17}_{-0.20}$	$49.1^{+5.2}_{-3.9}$	$0.66^{+0.08}_{-0.10}$	$2.2^{+0.5}_{-0.5}$	$3.3^{+0.6}_{-0.9}\times 10^{56}$	960^{+430}_{-410}	$0.19^{+0.07}_{-0.08}$	924
GW170608	$10.9^{+5.3}_{-1.7}$	$7.6^{+1.3}_{-2.1}$	$7.9^{+0.2}_{-0.2}$	$0.03^{+0.19}_{-0.07}$	$17.8^{+3.2}_{-0.7}$	$0.69^{+0.04}_{-0.04}$	$0.9^{+0.0}_{-0.1}$	$3.5^{+0.4}_{-1.3}\times 10^{56}$	320^{+120}_{-110}	$0.07^{+0.02}_{-0.02}$	396
GW170729	$50.6^{+16.6}_{-10.2}$	$34.3^{+9.1}_{-10.1}$	$35.7^{+6.5}_{-4.7}$	$0.36^{+0.21}_{-0.25}$	$80.3^{+14.6}_{-10.2}$	$0.81^{+0.07}_{-0.13}$	$4.8^{+1.7}_{-1.7}$	$4.2^{+0.9}_{-1.5}\times 10^{56}$	2750^{+1350}_{-1320}	$0.48^{+0.19}_{-0.20}$	1033
GW170809	$35.2^{+8.3}_{-6.0}$	$23.8^{+5.2}_{-5.1}$	$25.0^{+2.1}_{-1.6}$	$0.07^{+0.16}_{-0.16}$	$56.4^{+5.2}_{-3.7}$	$0.70^{+0.08}_{-0.09}$	$2.7^{+0.6}_{-0.6}$	$3.5^{+0.6}_{-0.9}\times 10^{56}$	990^{+320}_{-380}	$0.20^{+0.05}_{-0.07}$	340
GW170814	$30.7^{+5.7}_{-3.0}$	$25.3^{+2.9}_{-4.1}$	$24.2^{+1.4}_{-1.1}$	$0.07^{+0.12}_{-0.11}$	$53.4^{+3.2}_{-2.4}$	$0.72^{+0.07}_{-0.05}$	$2.7^{+0.4}_{-0.3}$	$3.7^{+0.4}_{-0.5}\times 10^{56}$	580^{+160}_{-210}	$0.12^{+0.03}_{-0.04}$	87
GW170817	$1.46^{+0.12}_{-0.10}$	$1.27^{+0.09}_{-0.09}$	$1.186^{+0.001}_{-0.001}$	$0.00^{+0.02}_{-0.01}$	≤ 2.8	≤ 0.89	≥ 0.04	$\geq 0.1\times 10^{56}$	40^{+10}_{-10}	$0.01^{+0.00}_{-0.00}$	16
GW170818	$35.5^{+7.5}_{-4.7}$	$26.8^{+4.3}_{-5.2}$	$26.7^{+2.1}_{-1.7}$	$-0.09^{+0.18}_{-0.21}$	$59.8^{+4.8}_{-3.8}$	$0.67^{+0.07}_{-0.08}$	$2.7^{+0.5}_{-0.5}$	$3.4^{+0.5}_{-0.7}\times 10^{56}$	1020^{+430}_{-360}	$0.20^{+0.07}_{-0.07}$	39
GW170823	$39.6^{+10.0}_{-6.6}$	$29.4^{+6.3}_{-7.1}$	$29.3^{+4.2}_{-3.2}$	$0.08^{+0.20}_{-0.22}$	$65.6^{+9.4}_{-6.6}$	$0.71^{+0.08}_{-0.10}$	$3.3^{+0.9}_{-0.8}$	$3.6^{+0.6}_{-0.9}\times 10^{56}$	1850^{+840}_{-840}	$0.34^{+0.13}_{-0.14}$	1651

Parameter estimation summary plots I. Posterior probability densities of the masses, spins, and SNR of the GW events. For the two-dimensional distributions, the contours show 90% credible regions. Left panel: Source frame component masses m1 and m2. We use the convention that m1 m2, which produces the sharp cut in the two-dimensional distribution. Lines of constant mass ratio q = m2=m1 are shown for 1=q = 2; 4; 8. For low-mass events, the contours follow lines of constant chirp mass. Right panel: The mass Mf and dimensionless spin magnitude af of the final black holes. The colored event labels are ordered by source frame chirp mass. The same color code and ordering (where appropriate) apply to Figs. 5 to 8.

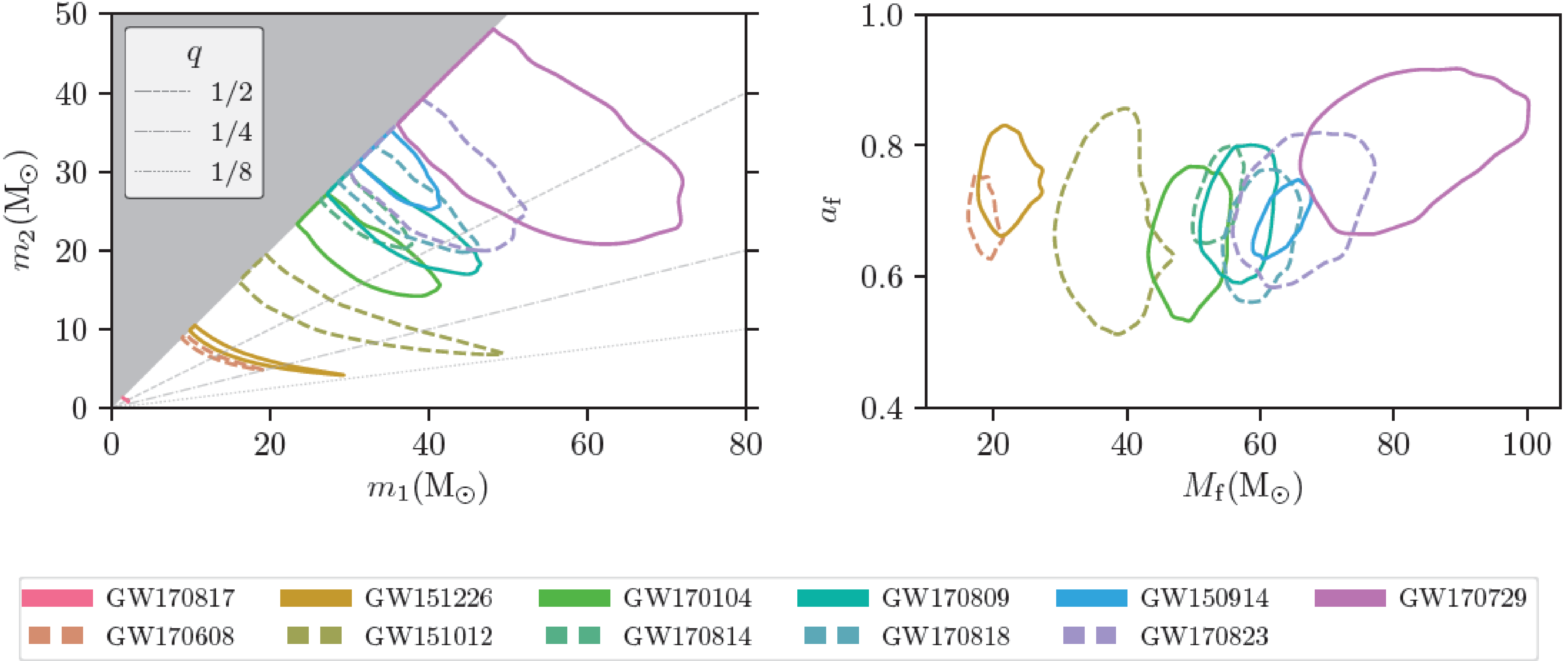

LVK Observation Scenario

- Possible KAGRA upgrade between O4 and O5

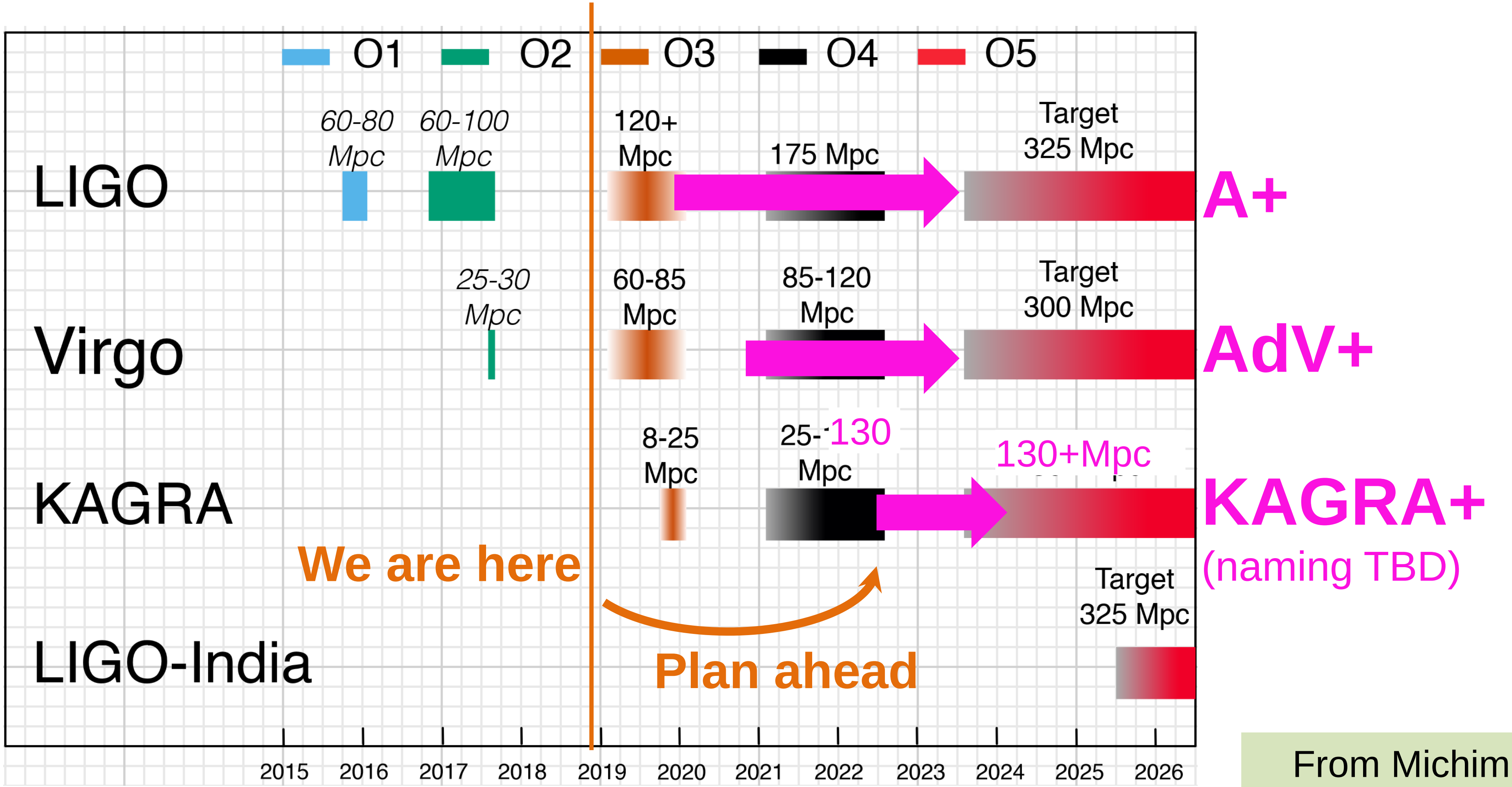

From Michimura

Modified from preliminary timeline from JRPC report 20180913
Approved by EO on Oct 17, 2018 ([JGW-T1809078]())

2G/2G+ Parameter Comparison

	KAGRA	AdVirgo	aLIGO	A+	Voyager
Arm length [km]	3	3	4	4	4
Mirror mass [kg]	23	42	40	80	200
Mirror material	Sapphire	Silica	Silica	Silica	Silicon
Mirror temp [K]	22	295	295	295	123
Sus fiber	35cm Sap.	70cm SiO_2	60cm SiO_2	60cm SiO_2	60cm Si
Fiber type	Fiber	Fiber	Fiber	Fiber	Ribbon
Input power [W]	67	125	125	125	140
Arm power [kW]	340	700	710	1150	3000
Wavelength [nm]	1064	1064	1064	1064	2000
Beam size [cm]	3.5 / 3.5	4.9 / 5.8	5.5 / 6.2	5.5 / 6.2	5.8 / 6.2
SQZ factor	0	0	0	6	8
F. C. length [m]	none	None	none	16	300

LIGO parameters from LIGO-T1600119, AdVirgo parameters from JPCS 610, 01201 (2015)

From Michimura

What next?

Earth-based

- ET 10 km arms 2030+
- Cosmic Explorer 2030+

  10 km, 20 km or 40 km

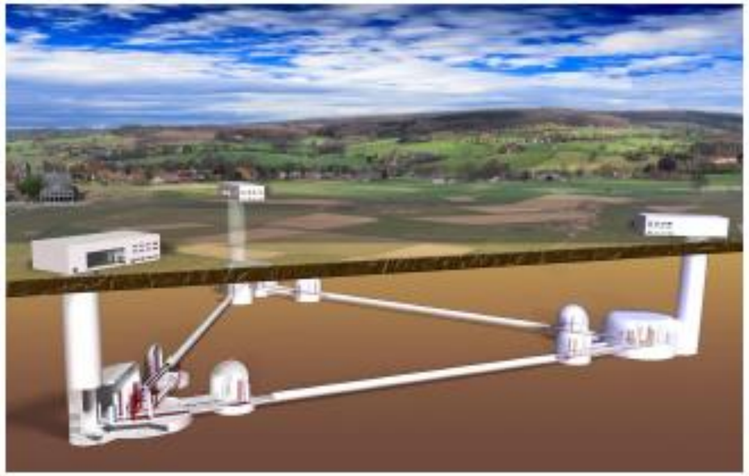

Space-borne

- LISA 2030+
- Other missions

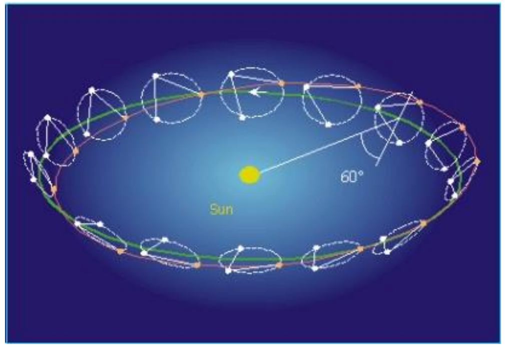

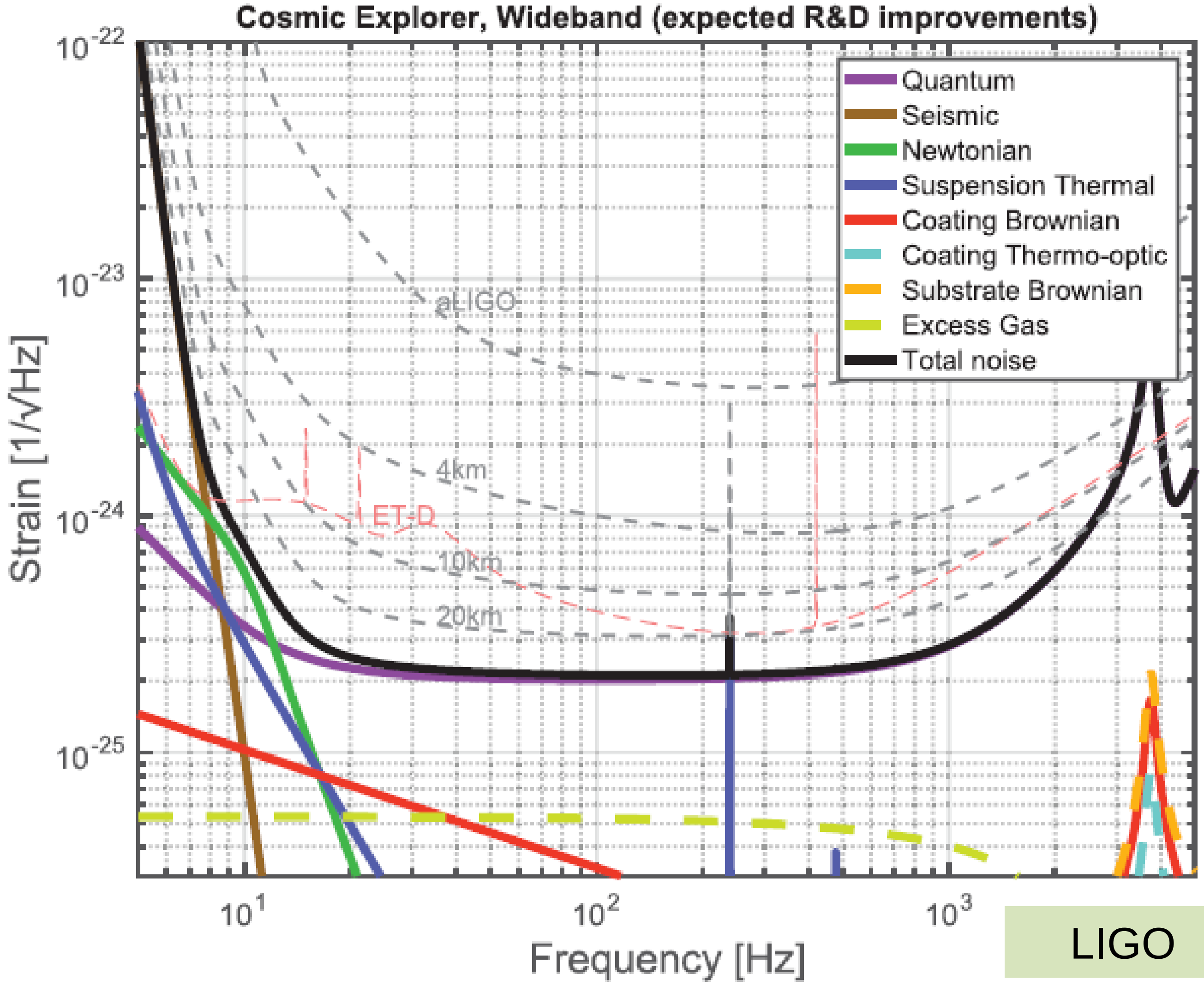

LIGO

Schematic of bKAGRA interferometer. All the mirrors shown are suspended inside the vacuum tanks with four types of vibration isolation systems. IMMT (OMMT): input (output) mode-matching telescope, IFI (OFI): input (output) Faraday isolator. Optics used in the Phase 1 operation are labeled in bold.

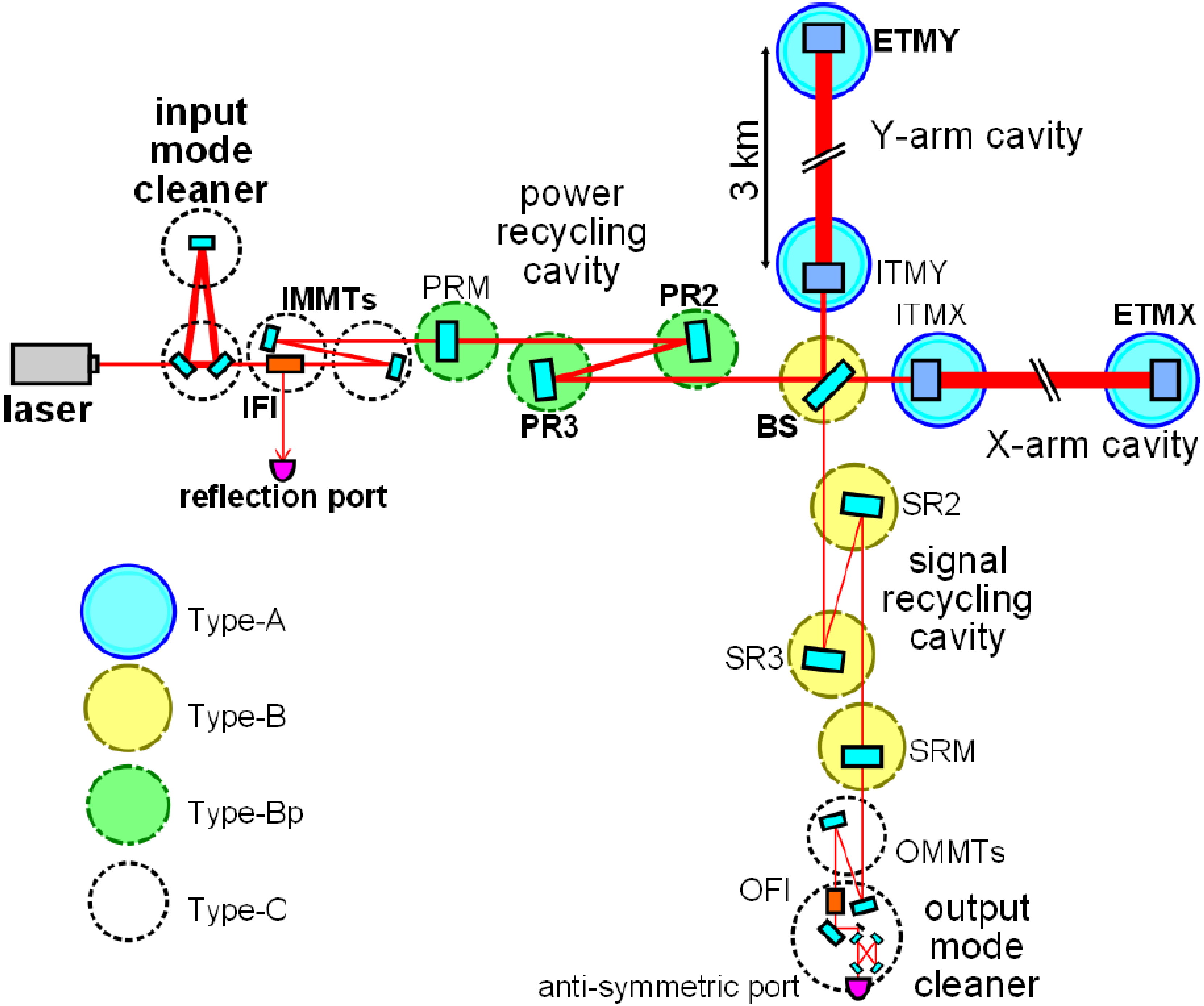

Figure 2. Four types of KAGRA mirror suspension system. Type-A system is for
ITMs and ETMs. Type-B system is for BS and signal recycling mirrors. Type-Bp
system is for power recycling mirrors. Type-C system is used for other auxiliary
mirrors.

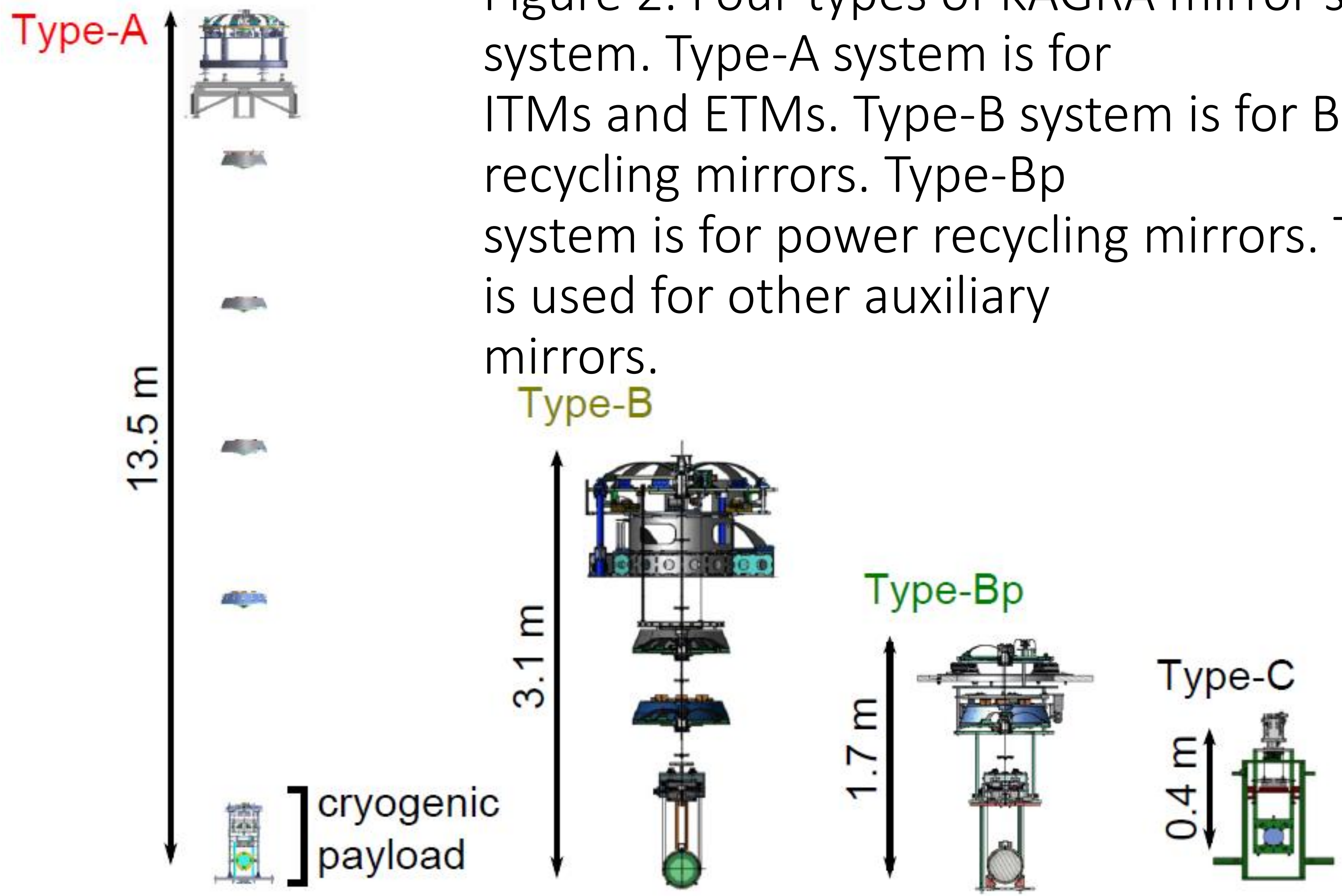

CAD drawing of the cryogenic payload (left) and the schematic of the cryogenic suspension system of sapphire test masses (right).

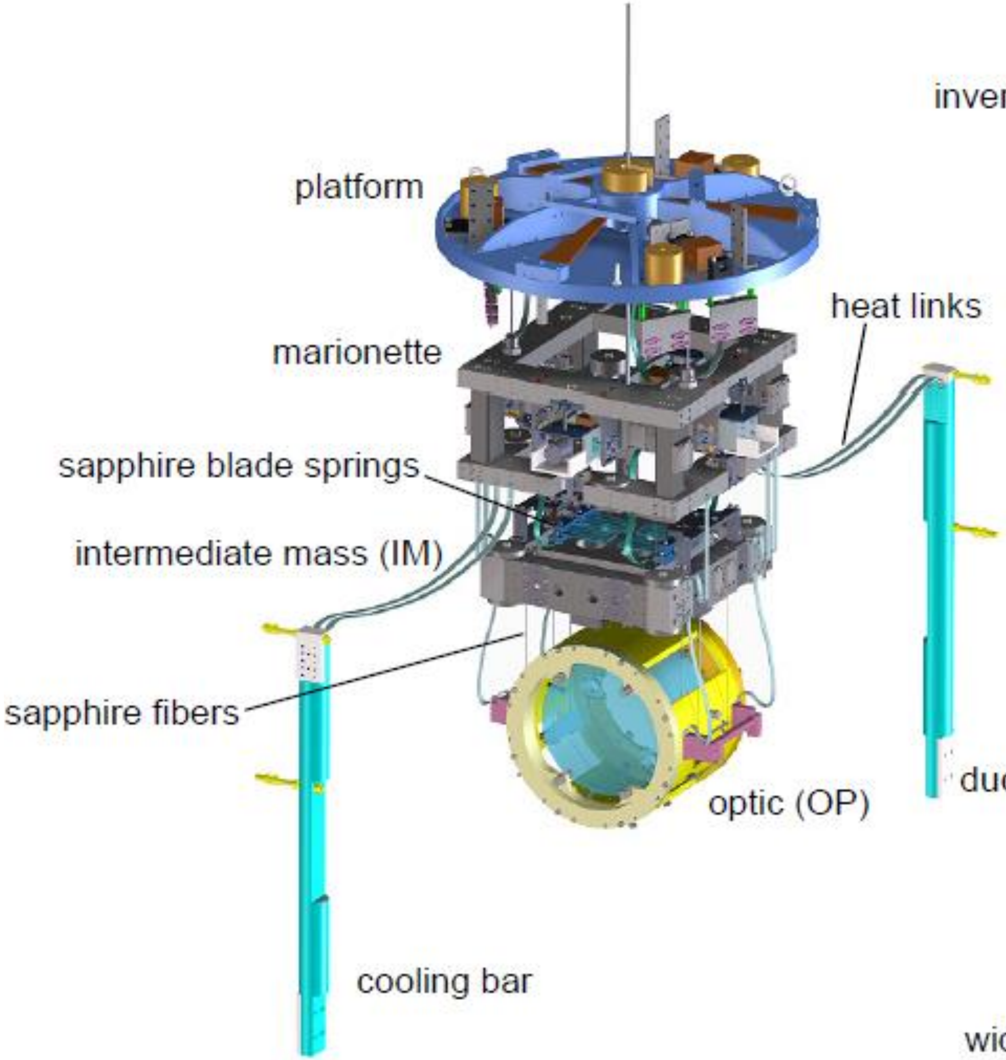

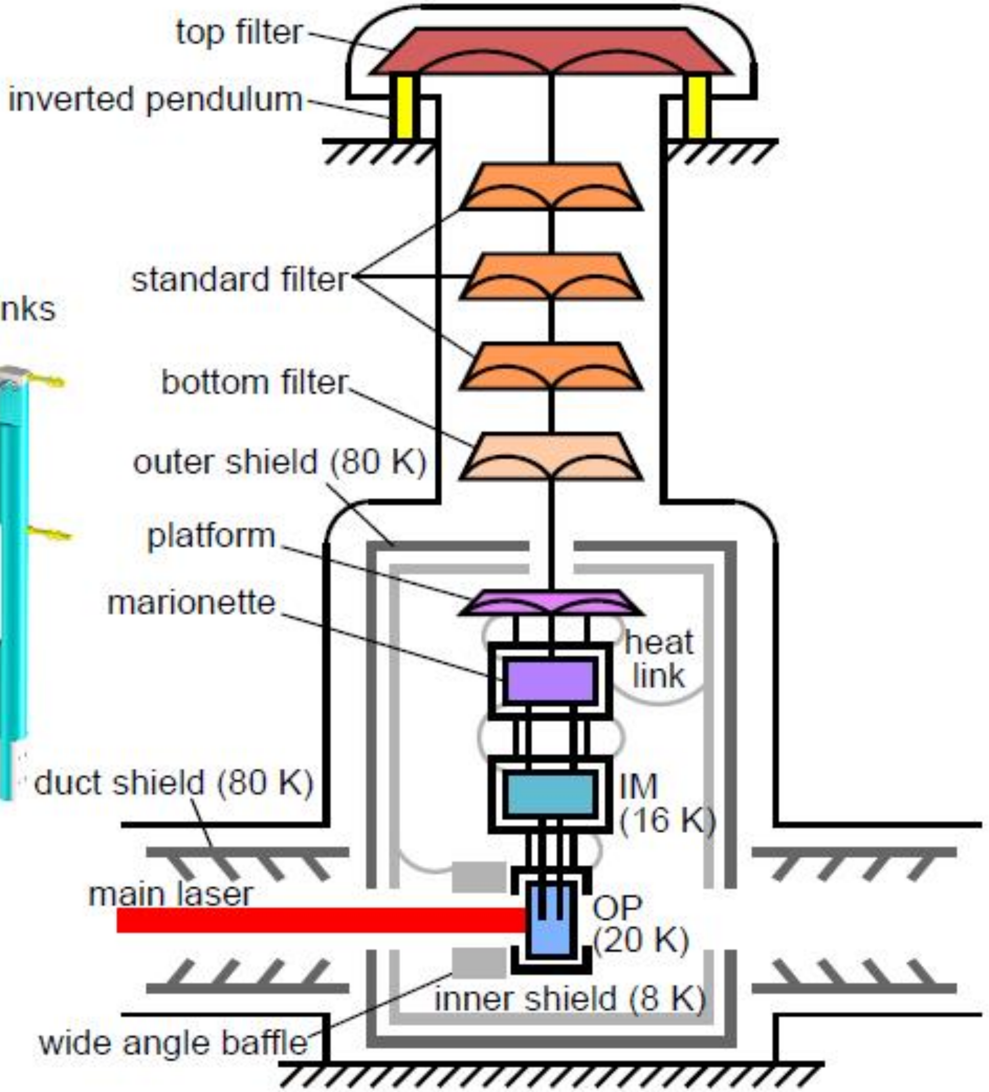

KAGRA

Feasibility Study: Heavier Mirror

- Larger sapphire bulk available, but requires R&D for polishing and coating, needs time and money
  - φ 55 cm x t 30 cm (~280 kg) mirror would be possible in the future
  - Current one (φ 22 cm x t 15 cm, 23 kg) more than 1 year to polish, $0.6M / mirror
  - Current cryostat is quite full (40 kg at most?)

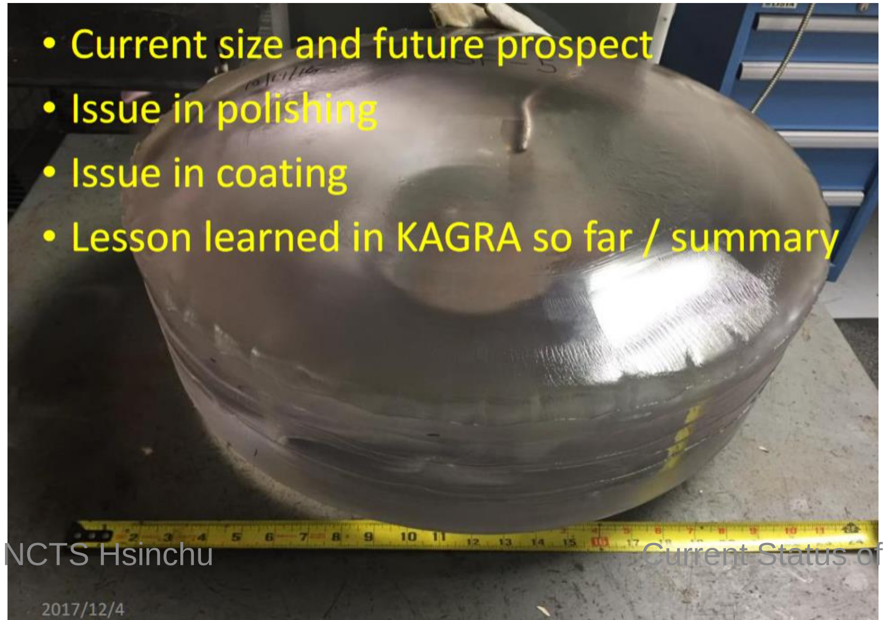

[K. Somiya, JGW-G1808231]

[E. Hirose JGW-G1707484]

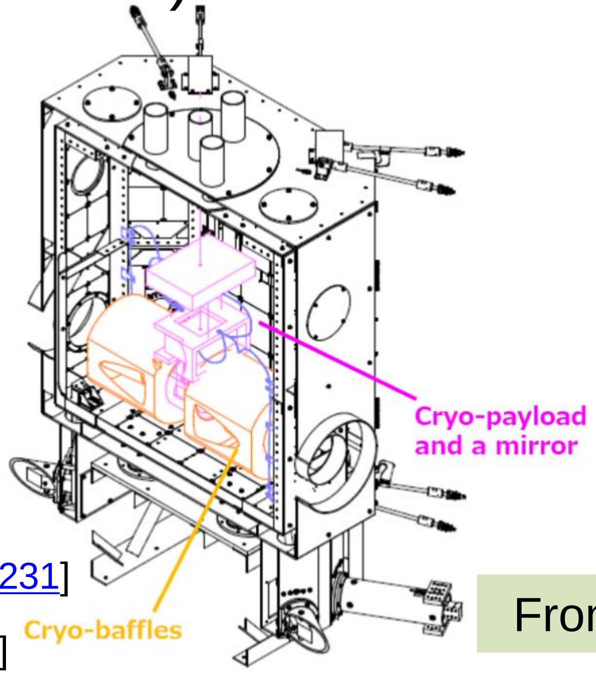

From Michimura

Feasibility Study: High Power

- Higher power laser source at 400 W would be available, but operation is tough
  - thermal compensation
  - parametric instability
  - radiation pressure induced instability etc…
- Could be OK with cryogenic sapphire?

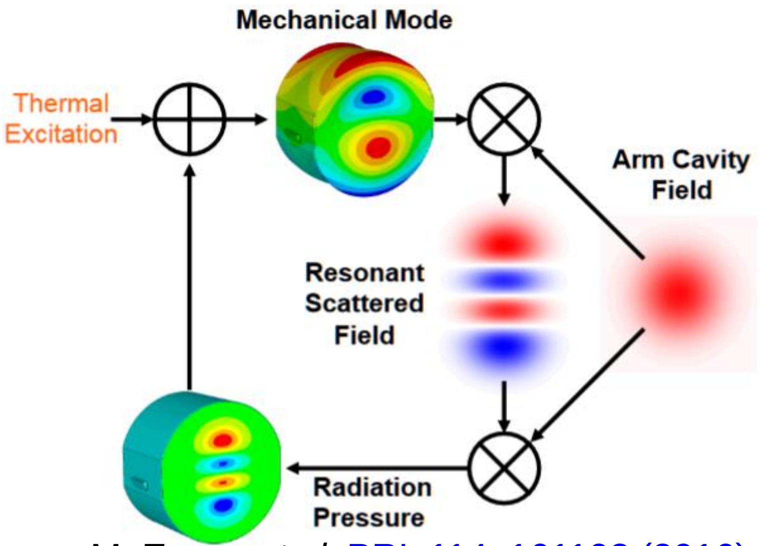

M. Evans *et al*, PRL 114, 161102 (2016)

S. Fu *et al*, JOSA B 34, A49 (2017)

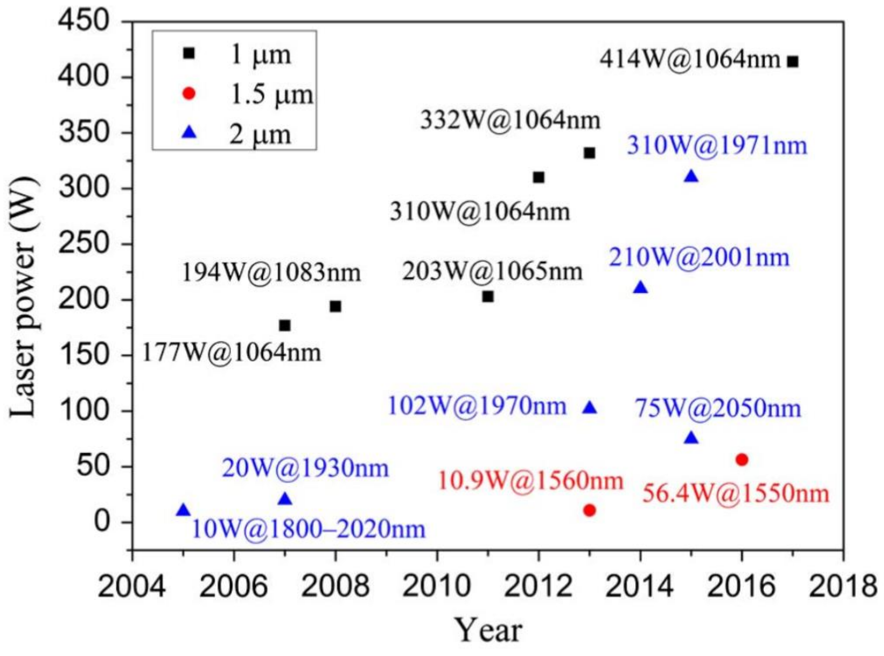

Fig. 7. Output power evolution of CW single-frequency amplifiers in all-fiber format operating in 1, 1.5, and 2 μm regions.

From Michimura

Feasibility Study: Filter Cavity

- One core optic per tank, not very crowded
- ~30 m could be OK, but >100 m would require new vacuum tube

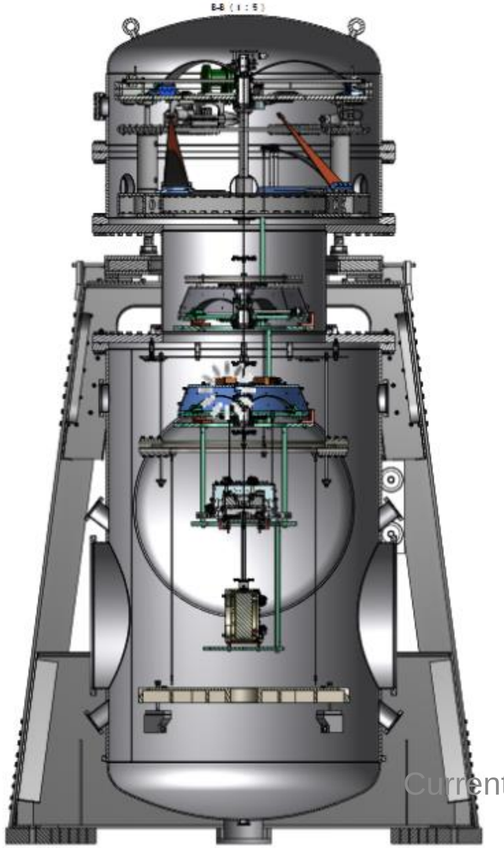

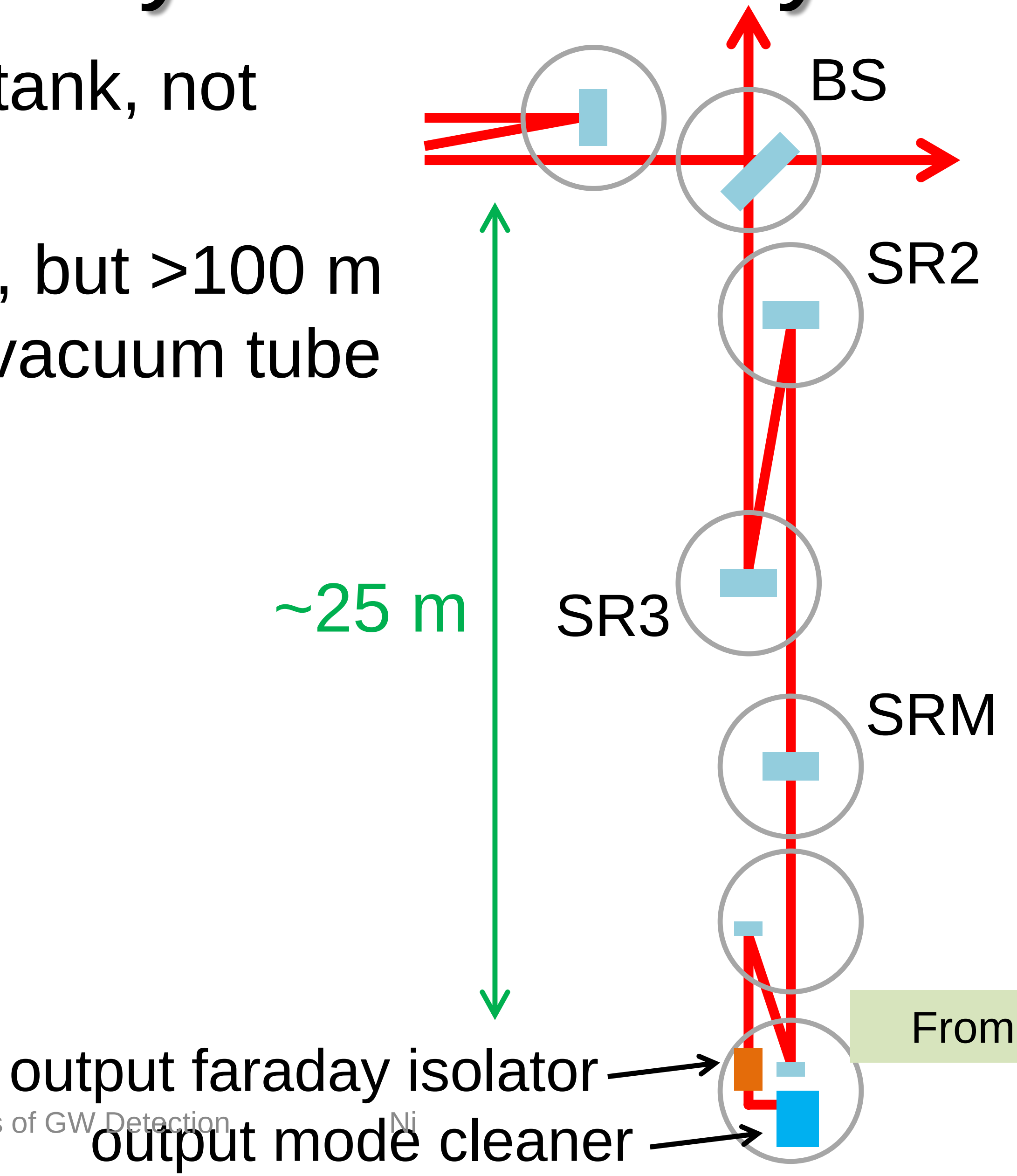

From Michimura

GW20150914

LIGO

LISA

(from Sesana 2017 prl)

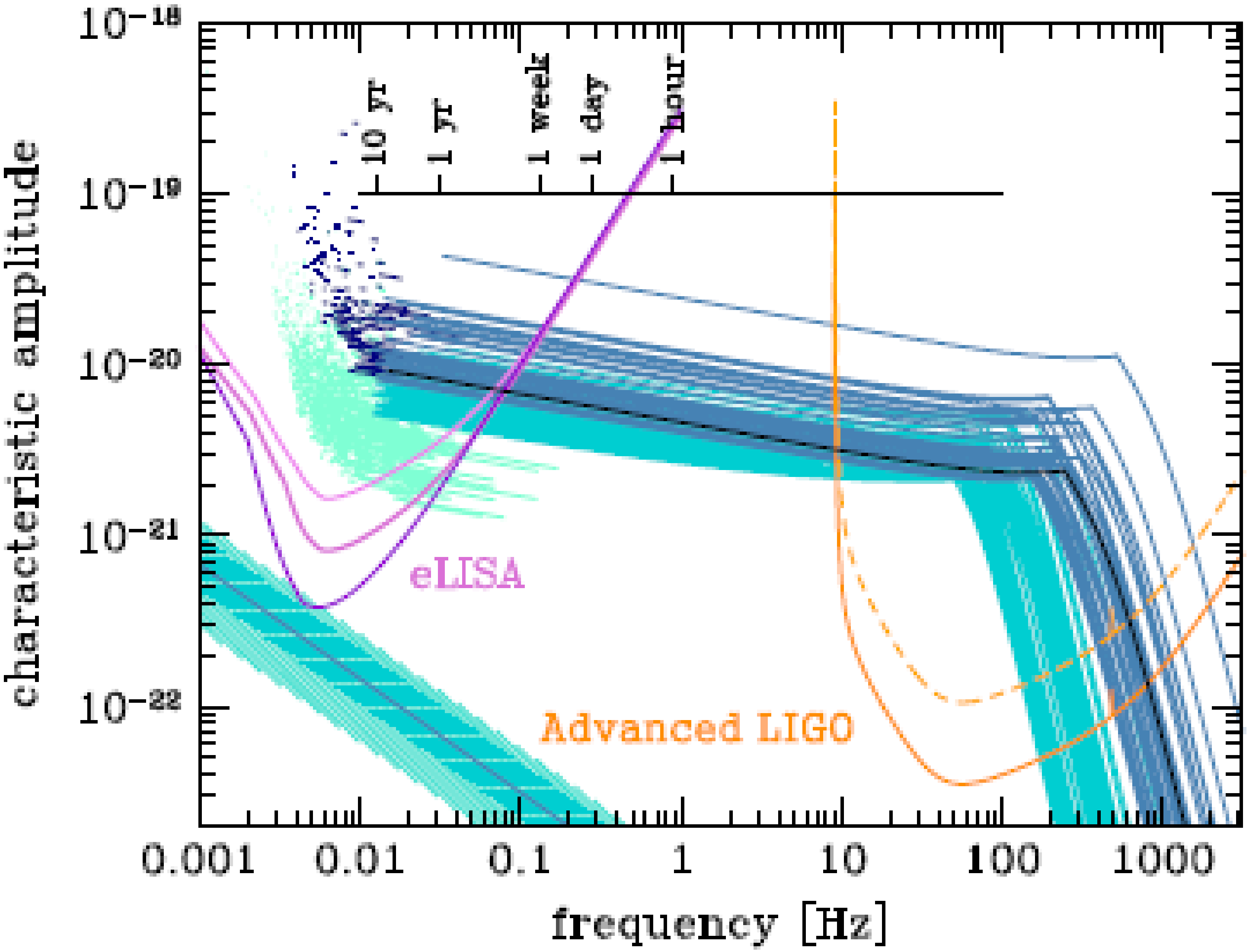

Torsion-Bar Antenna for Low-Frequency Gravitational-Wave Observations

Masaki Ando,[1,*] Koji Ishidoshiro,[2,†] Kazuhiro Yamamoto,[3] Kent Yagi,[1] Wataru Kokuyama,[2]
Kimio Tsubono,[2] and Akiteru Takamori[4]

- TOBA – The torsion bar antenna; PRL2010, PRD2013
- 10 m x 0.6 m ϕ quartz/Al 5056
- 10 ton each
- Fundamental torsion frequency 30 μHz

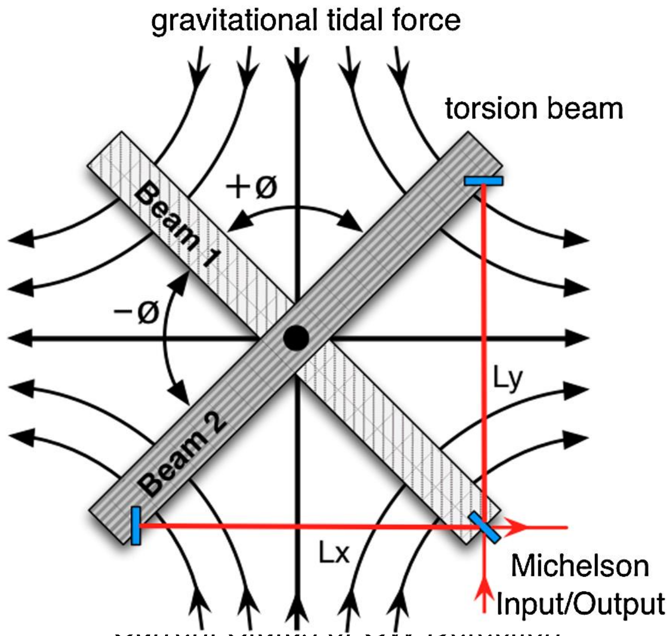

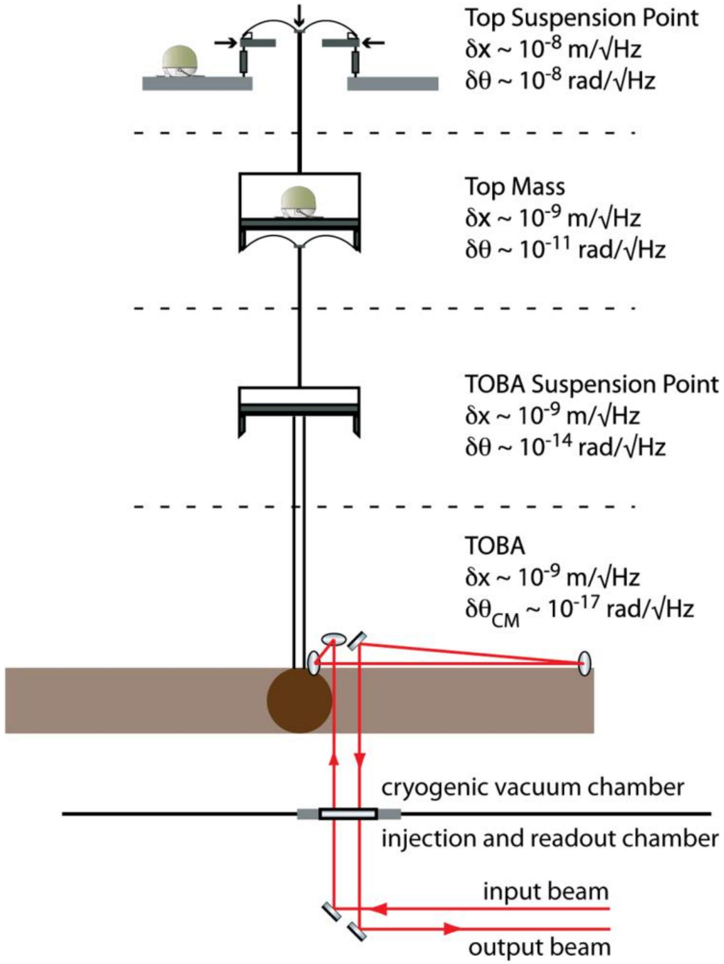

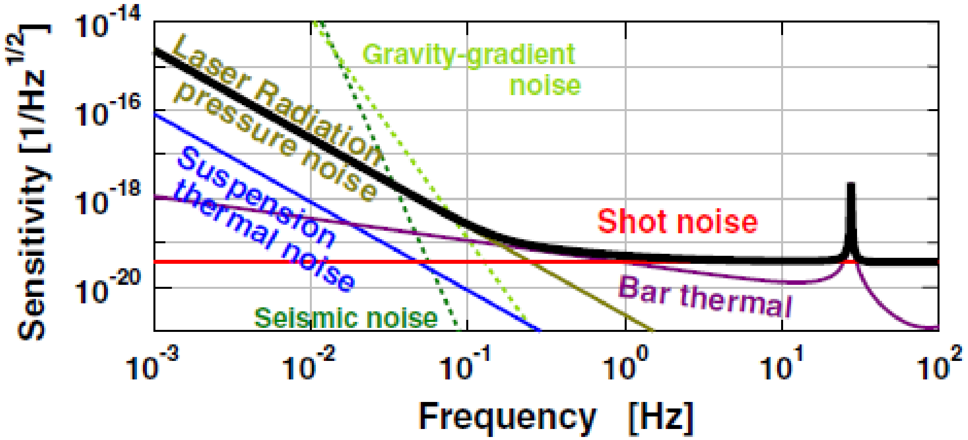

FIG. 2 (color online). Estimated sensitivity of a torsion-bar antenna (thick black curve). Limitations by fundamental noises are shown together.

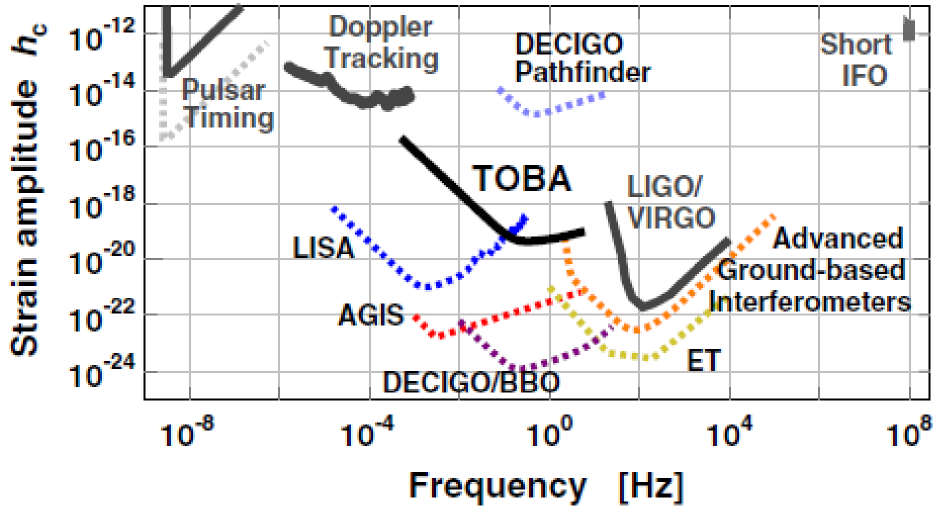

Newtonian Noise – seismic and atmospheric NN would have to be reduced by large factors to achieve sensitivity goals with respect of NN

It is uncertain whether sufficiently sensitive seismic and infrasound sensors can be provided. It will be very challenging to achieve sufficient NN subtraction. A suppression of the NN by about 4 or 5 orders of magnitude at 0.1 Hz would be needed to make it comparable to the instrument noise limit. A larger number of more sensitive sensors will be required.

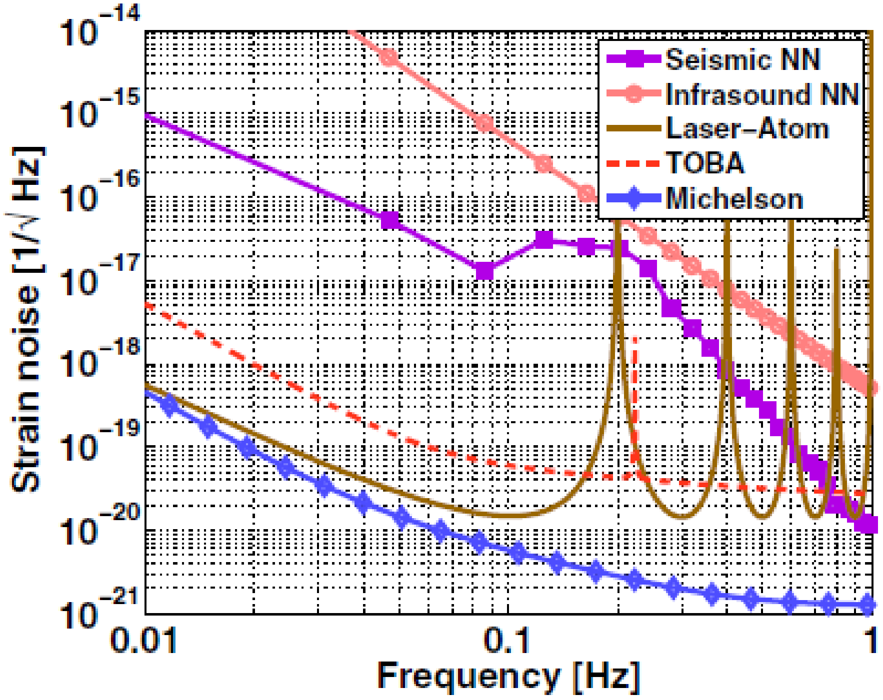

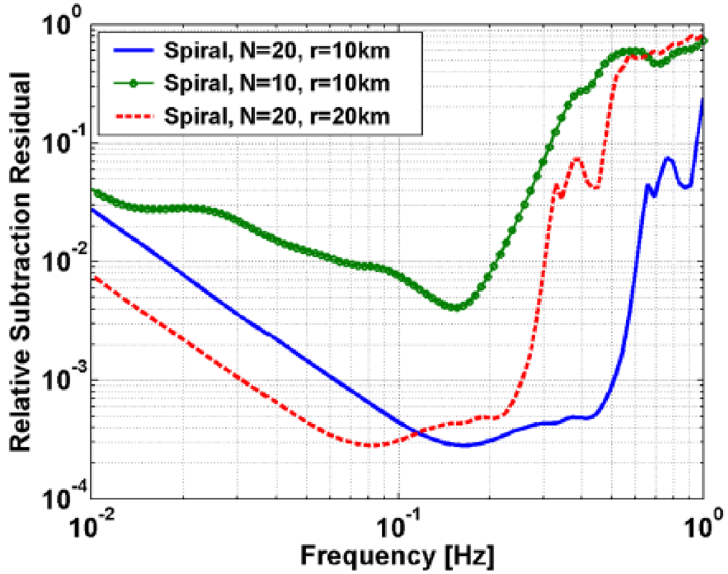

FIG. 10 (color online). Residuals of Rayleigh-wave gradient NN subtraction for double-wound spiral arrays using seismometers with SNR = 1000. Results are presented for different numbers N of seismometers and different array radii r.

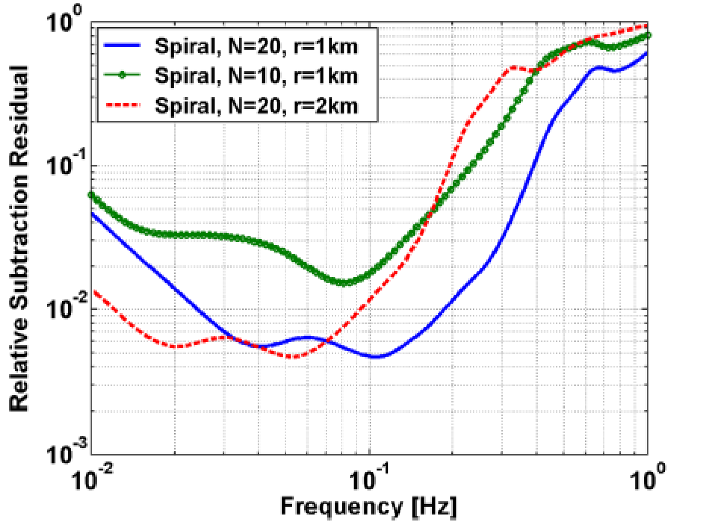

FIG. 11 (color online). Residuals of infrasound gradient NN subtraction for double-wound spiral arrays using microphones with SNR = 1000. Results are presented for different numbers N of microphones and different array radii r.

Harms et al

SOGRO (Paik et al 2016)
(Superconducting Omni-directional Gravitational Radiation Observatory)

A design concept that could reach a strain sensitivity of 10^{-19}–10^{-20} $Hz^{-1/2}$ at 0.2–10 Hz

the range of the WD–WD binary from 0.1 Hz for one year with a SNR of 10 is 1.2 Mpc, assuming one solar mass ($M_\odot$) for the WD mass. Within this horizon, there are two massive galaxies: the Milky Way Galaxy and Andromeda (M31). The WD–WD merger rate of $\sim 1.4\times10^{-13}$ $yr^{-1}M_\odot^{-1}$ has been estimated, corresponding to 0.01 per year for our Galaxy. With M31 about 0.03 per year. Probability of finding a WD–WD binary merger during one-year operation of SOGRO is ~30% since each event is expected to persist for ~10 years in the detector.

Binary mergers composed of IMBHs can be detected by SOGRO up to several Gpc (see figure 1). The estimated rates of mergers are very uncertain, but up to a few tens of IMBH mergers can be detected per year by SOGRO [7].

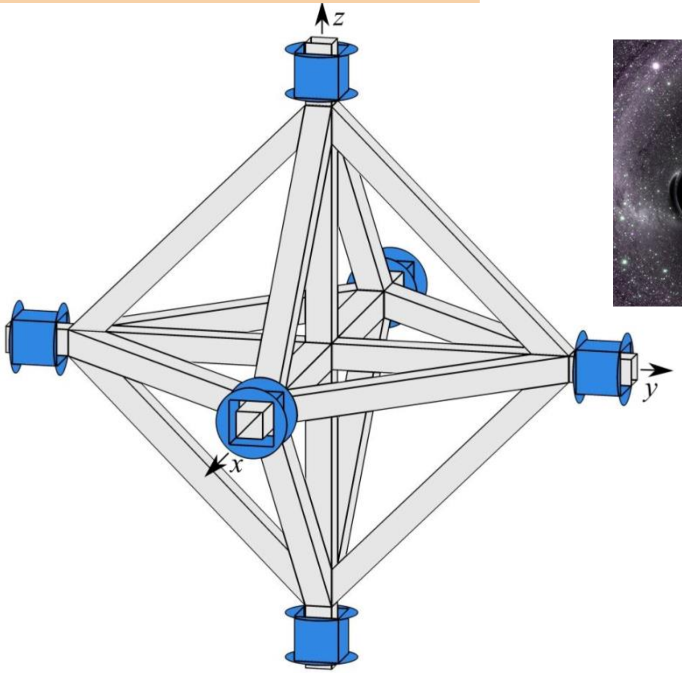

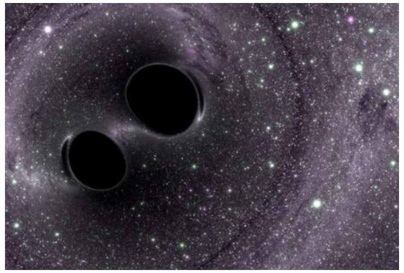

Each test mass M 5 ton Nb square tube
Arm length L 30-50 m Over a 'rigid' platform
Antenna temperature T 1.5 K Superfluid helium or cryocoolers
DM quality factor 5×10^8 Surface-polished pure Nb
Signal frequency f 0.1–10 Hz

Ho Jung Paik
Department of Physics, University of Maryland

ICGAC-XIII, Seoul, July 4, 2017

Exploring gravity with the MIGA large scale atom interferometer

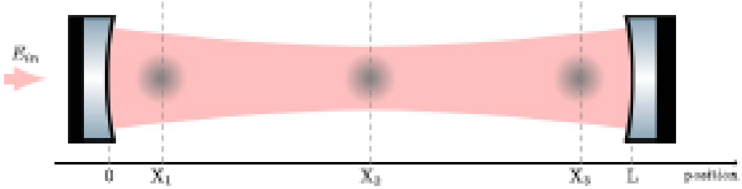

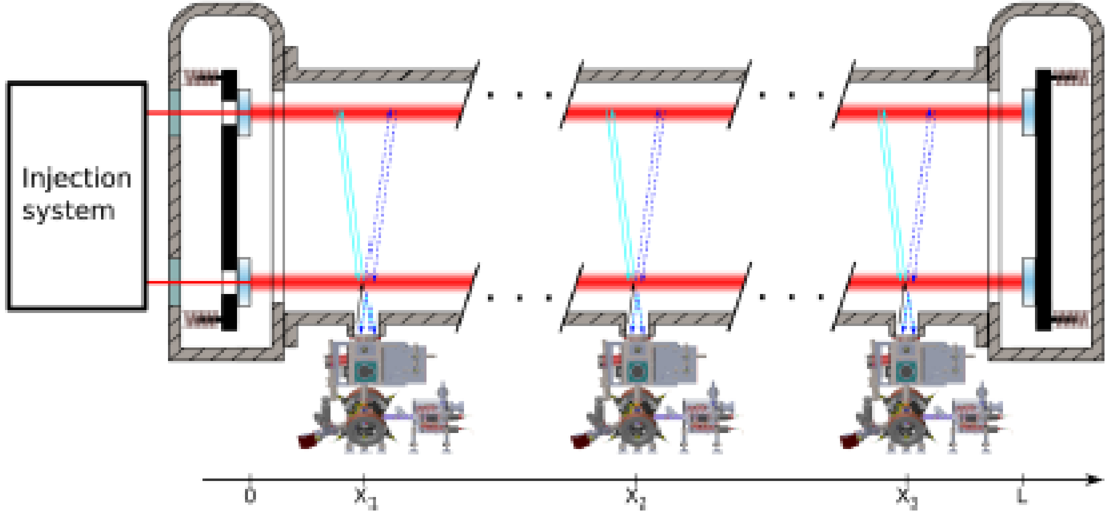

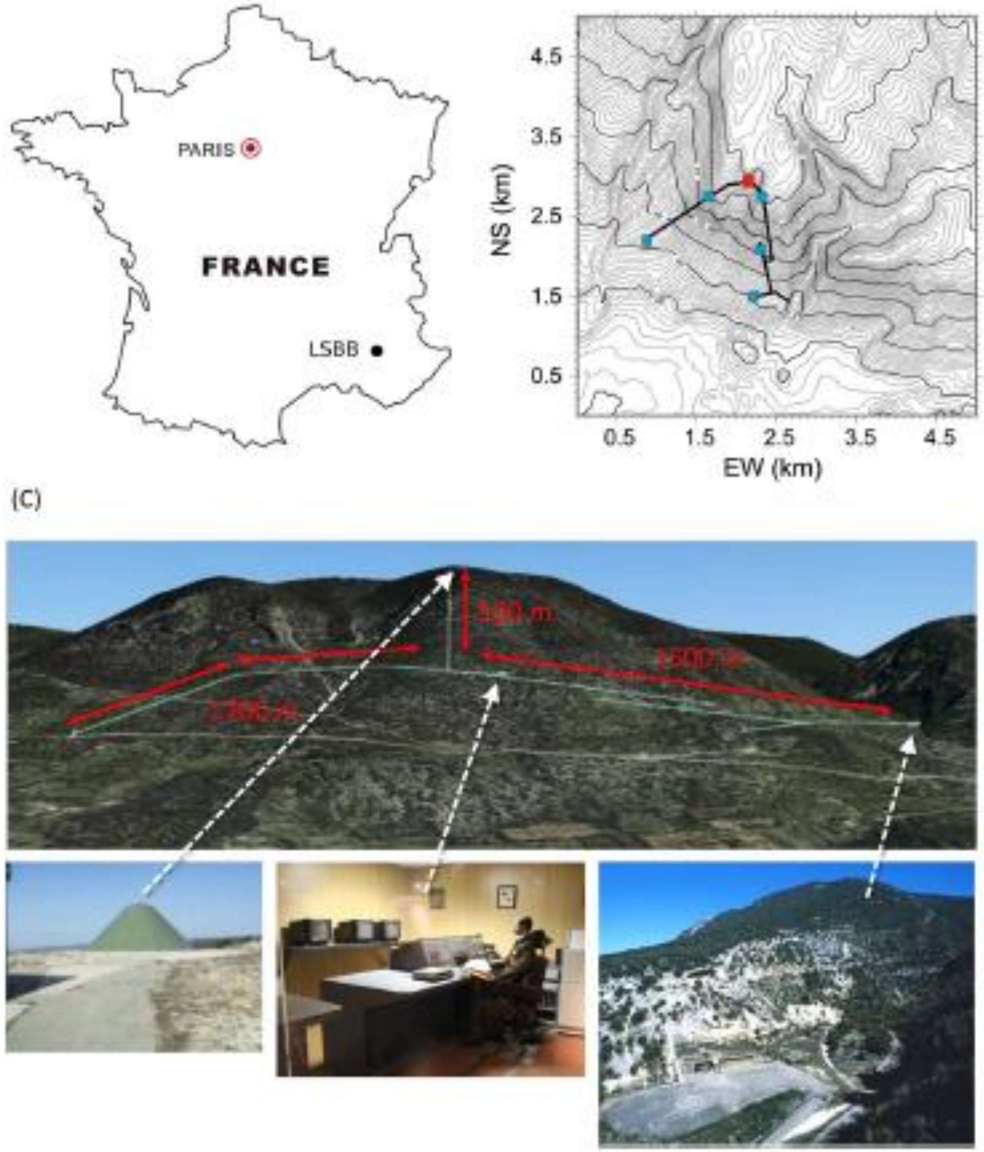

Equipment needed for Gravity
(from FOMO presentation by J Wang and MS Zhan)

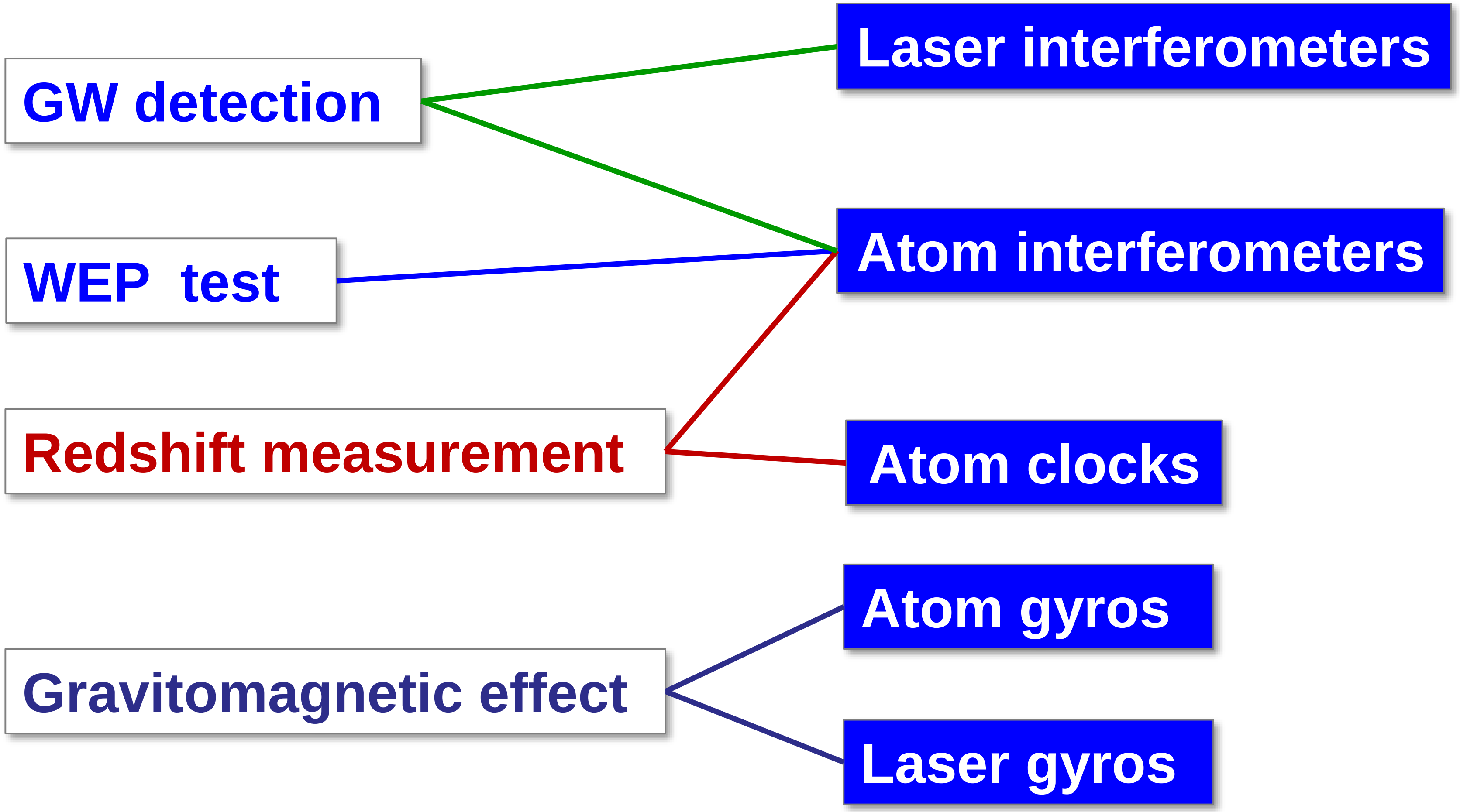

ZAIGA facility

ZAIGA facility proposal, Wuhan Institute of Physics and Mathematics, Chinese Academy of Sciences, Wuhan

Zhaoshan long-baseline **A**tom **I**nterferometer **G**ravitation **A**ntenna

ZAIGA design renderings

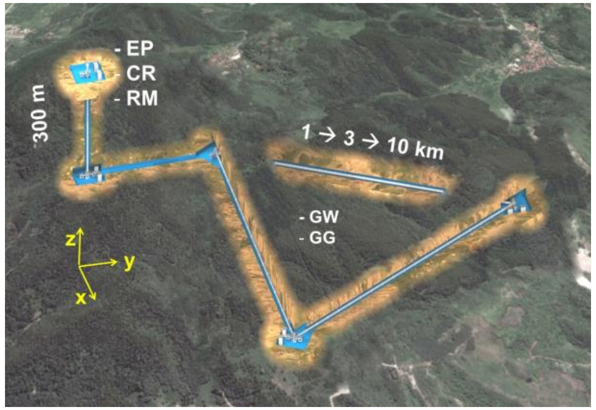

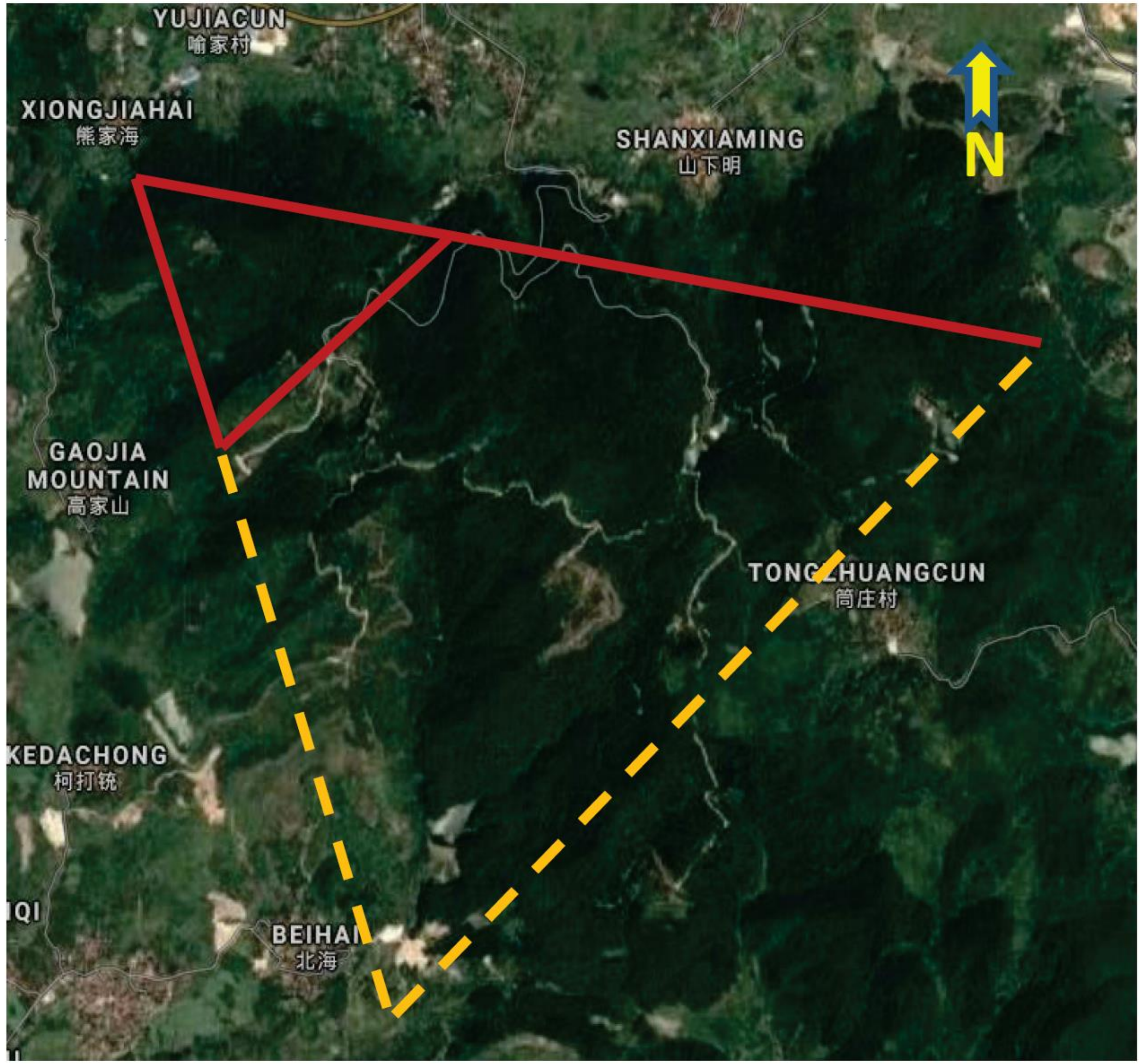

Where is Wuhan ?

ZAIGA facility

An underground facility for GR tests using large scale atom interferometers, gyros and clocks

- **ZAIGA-GW (Gravitation Wave detection)**
- **ZAIGA-EP (Equivalence Principle test)**
- **ZAIGA-CE (Redshift measurement, GW prototype)**
- **ZAIGA-RM (Rotation Measurement)**
- **ZAIGA-GG (Geological and Geophysical measurement)**

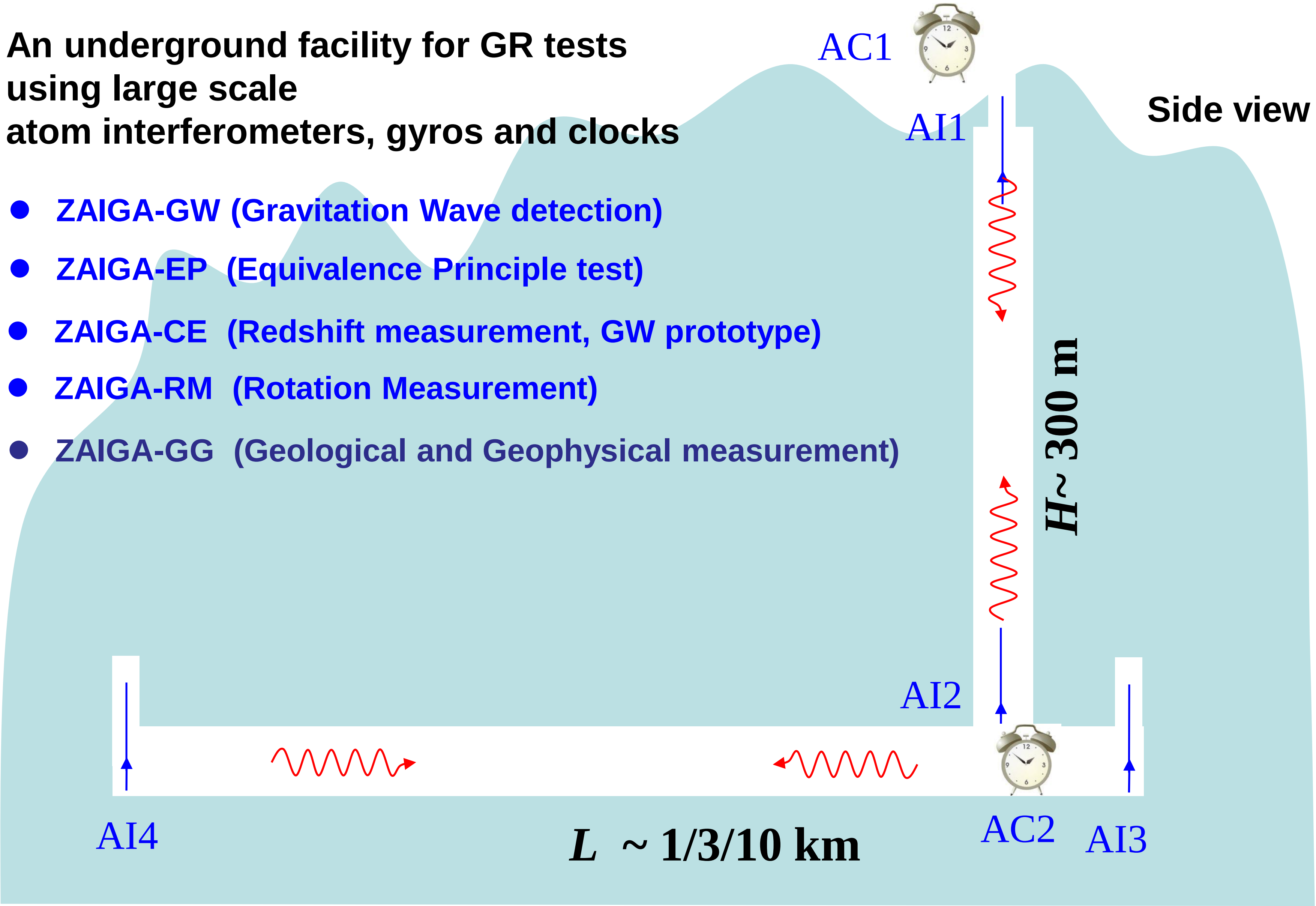

Personnel

ZAIGA-GW


Ming-Sheng Zhan


Wei-Tou Ni


Dong-Feng Gao

ZAIGA-EP


Jin Wang


Lin Zhou


Xi Chen

ZAIGA-RM


Run-Bing Li


Zhan-Wei Yao


Jia-Qi Zhong

ZAIGA-CR


Ling-Xiang He


Zong-Yuan Xiong

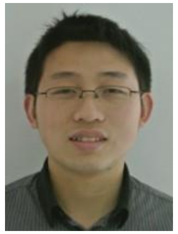
Biao Tang

Comparison of arm length

< 50 km, Earth
> 100 km, Space

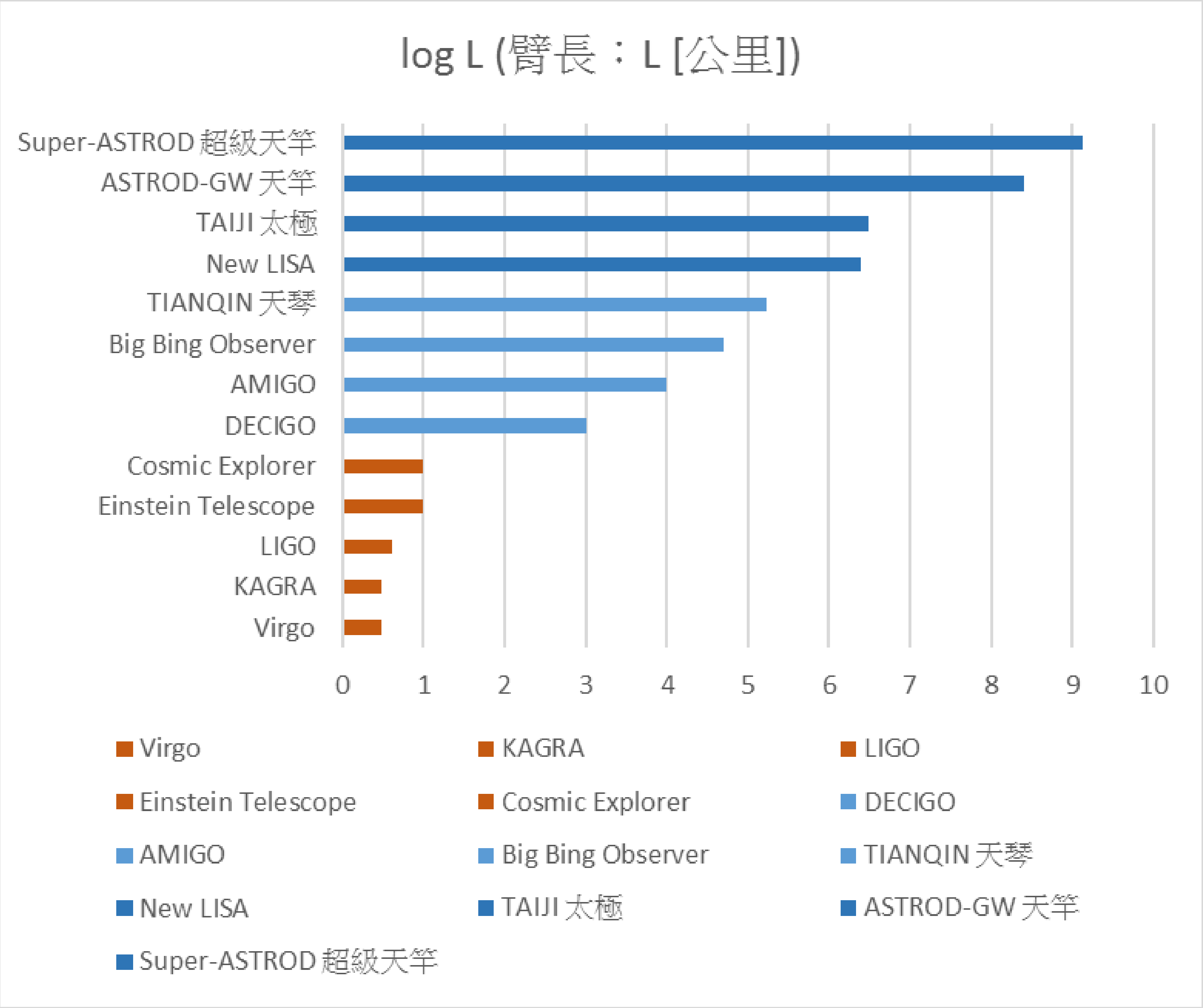

引力波谱分类 The Gravitation-Wave (GW) Spectrum Classification

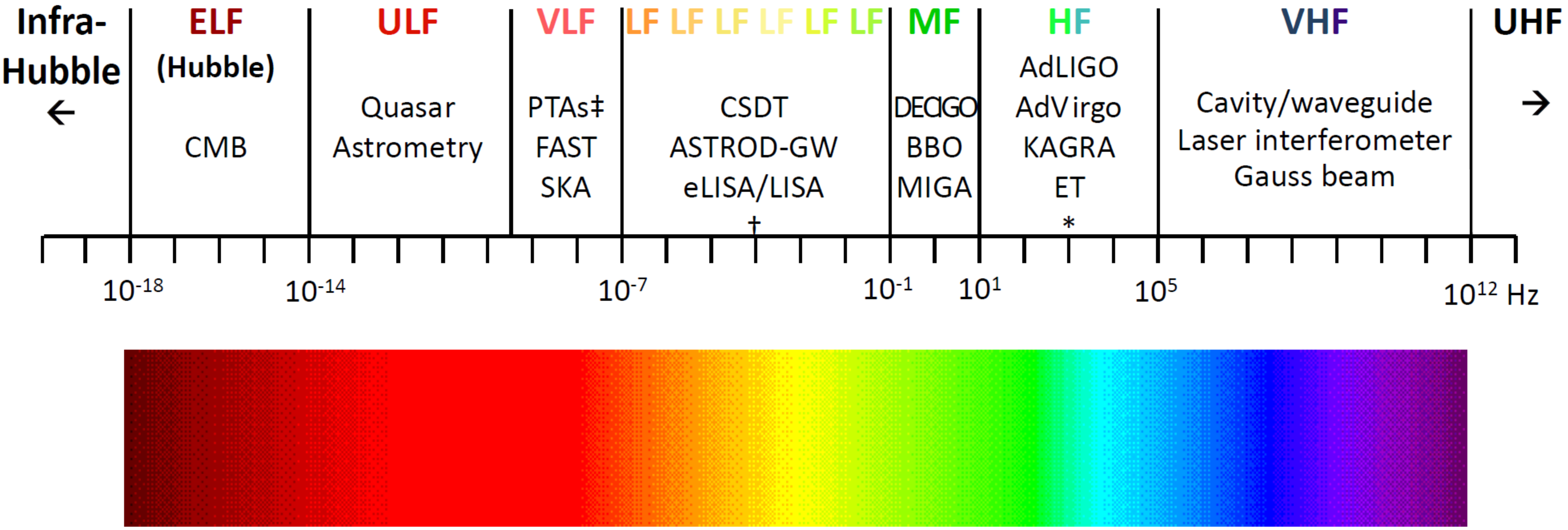

* AIGO, AURIGA, EXPLORER, GEO, NAUTILUS, MiniGRAIL, Schenberg.

† OMEGA, gLISA/GEOGRAWI, GADFLI, TIANQIN, ASTROD-EM, LAGRANGE, ALIA, ALIA-descope.

‡ EPTA, NANOGrav, PPTA, IPTA.

Normalized GW spectral energy density Ω_{gw} vs. frequency for GW detector sensitivities and GW sources

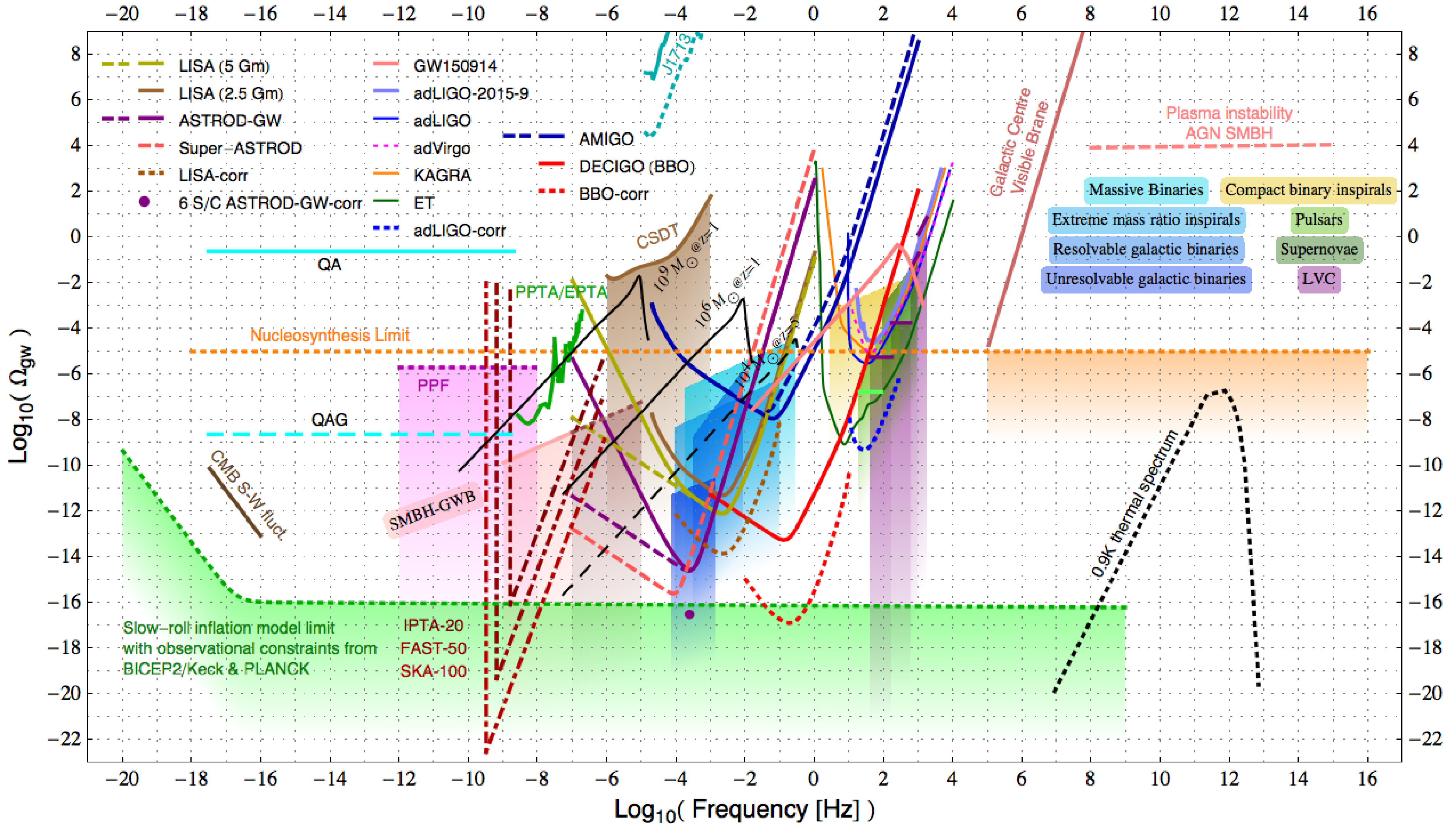

Pulsar Timing Arrays

PPTA, NANOGrav, EPTA, IPTA
FAST, SKA

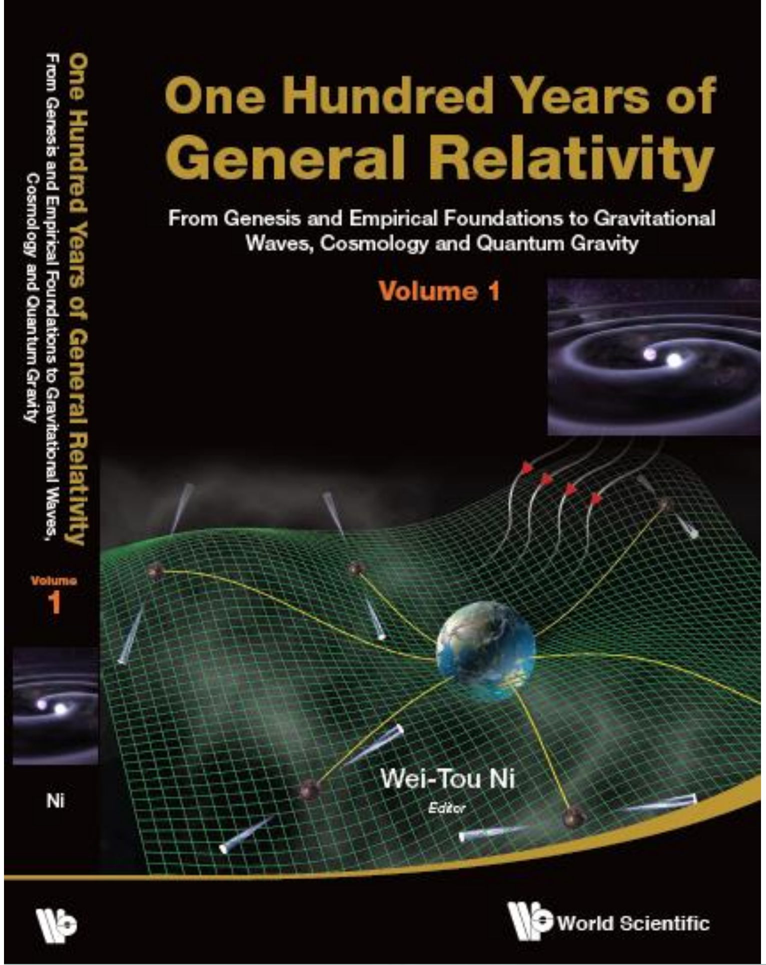

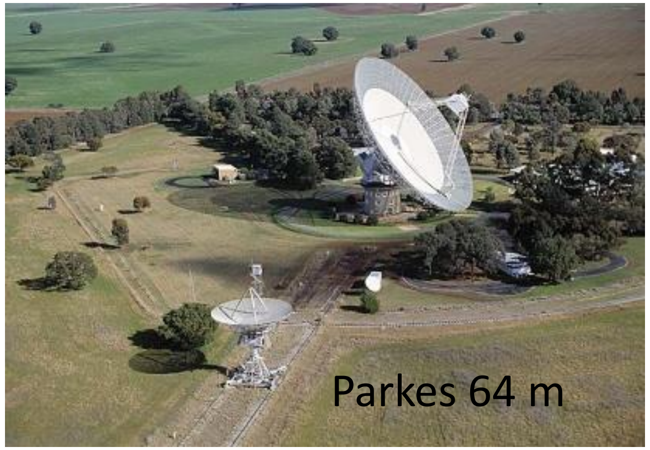

Parkes 64 m

Effelsberg 100 m

Arecibo 300 m

SKA Pathfinder

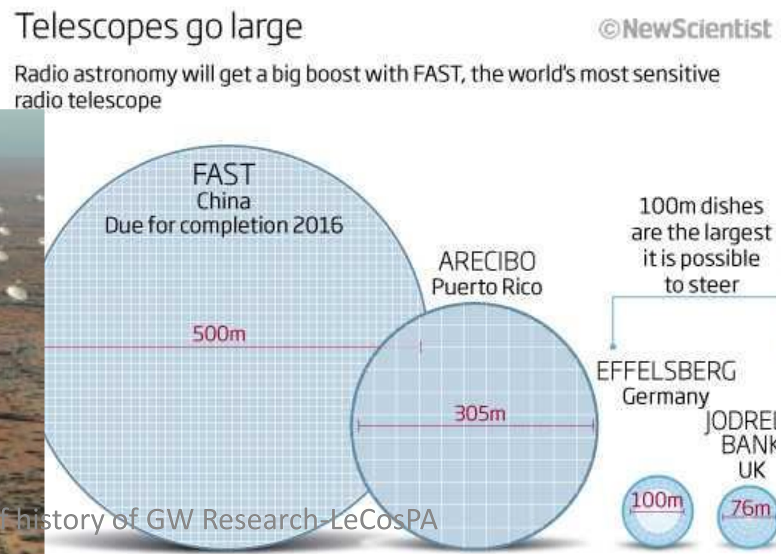

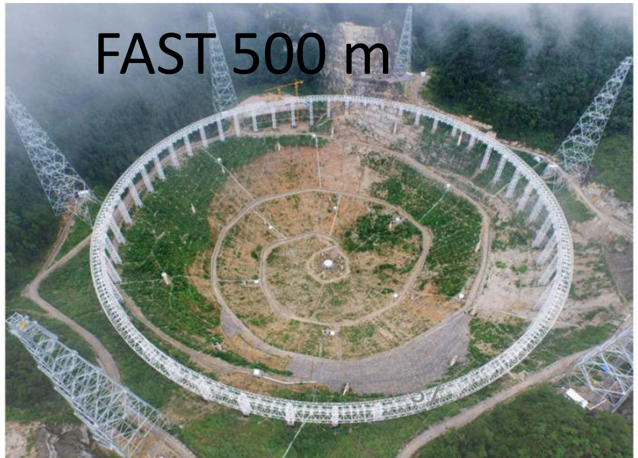

FAST 500 m

Summary and Outlook

- 10 BBH events up to cosmological distance: 9 Gly (z=0.5) & 1 BNS event are observed (40 Mpc).
- Detection efforts have been made in all frequency bands; CMB polarization observation are also vigorously proceeded to search for tensor imprints.
- GW detection will play a dominating role in Astronomy and Cosmology in next 50 years.

Thank you

Scope: Goals –GW Astronomy & Fundamental Physics

Frequency band	GW sources / Possible GW sources	Detection method
Ultrahigh frequency band: above 1 THz	Discrete sources, Cosmological sources, Braneworld Kaluza-Klein (KK) mode radiation, Plasma instabilities	Terahertz resonators, optical resonators, and magnetic conversion detectors
Very high frequency band: 100 kHz – 1 THz	Discrete sources, Cosmological sources, Braneworld Kaluza-Klein (KK) mode radiation, Plasma instabilities	Microwave resonator/wave guide detectors, laser interferometers and Gaussian beam detectors
High frequency band (audio band)*: 10 Hz – 100 kHz	Compact binaries [NS (Neutron Star)-NS, NS-BH (Black Hole), BH-BH], Supernovae	Low-temperature resonators and Earth-based laser-interferometric detectors
Middle frequency band: 0.1 Hz – 10 Hz	Intermediate mass black hole binaries, massive star (population III star) collapses	Space laser-interferometric detectors of arm length 1,000 km – 60,000 km
Low frequency band (milli-Hz band)†: 100 nHz – 0.1 Hz	Massive black hole binaries, Extreme mass ratio inspirals (EMRIs), Compact binaries	Space laser-interferometric detectors of arm length longer than 60,000 km
Very low frequency band (nano-Hz band): 300 pHz – 100 nHz	Supermassive black hole binary (SMBHB) coalescences, Stochastic GW background from SMBHB coalescences	Pulsar timing arrays (PTAs)
Ultralow frequency band: 10 fHz – 300 pHz	Inflationary/primordial GW background, Stochastic GW background	Astrometry of quasar proper motions
Extremely low (Hubble) frequency band: 1 aHz–10 fHz	Inflationary/primordial GW background	Cosmic microwave background experiments
Beyond Hubble-frequency band: below 1 aHz	Inflationary/primordial GW background	Through the verifications of primordial cosmological models